



AERO. & ASTRO. LIBRARY

Dr. Hunsaker

# NATIONAL ADVISORY COMMITTEE FOR AERONAUTICS

REPORT No. 590

*Copy # 3*

## PRESSURE-DISTRIBUTION MEASUREMENTS ON AN O-2H AIRPLANE IN FLIGHT

By H. A. PEARSON



1937



# AERONAUTIC SYMBOLS

## 1. FUNDAMENTAL AND DERIVED UNITS

	Symbol	Metric		English	
		Unit	Abbrevia- tion	Unit	Abbrevia- tion
Length-----	$l$	meter-----	m	foot (or mile)-----	ft. (or mi.)
Time-----	$t$	second-----	s	second (or hour)-----	sec. (or hr.)
Force-----	$F$	weight of 1 kilogram-----	kg	weight of 1 pound-----	lb.
Power-----	$P$	horsepower (metric)-----		horsepower-----	hp.
Speed-----	$V$	{kilometers per hour----- meters per second-----	{k.p.h. m.p.s.	{miles per hour----- feet per second-----	{m.p.h. f.p.s.

## 2. GENERAL SYMBOLS

$W$ ,	Weight = $mg$	$\nu$ ,	Kinematic viscosity
$g$ ,	Standard acceleration of gravity = 9.80665 m/s <sup>2</sup> or 32.1740 ft./sec. <sup>2</sup>	$\rho$ ,	Density (mass per unit volume)
$m$ ,	Mass = $\frac{W}{g}$		Standard density of dry air, 0.12497 kg-m <sup>-4</sup> -s <sup>2</sup> at 15° C. and 760 mm; or 0.002378 lb.-ft. <sup>-4</sup> sec. <sup>2</sup>
$I$ ,	Moment of inertia = $mk^2$ . (Indicate axis of radius of gyration $k$ by proper subscript.)		Specific weight of "standard" air, 1.2255 kg/m <sup>3</sup> or 0.07651 lb./cu.ft.
$\mu$ ,	Coefficient of viscosity		

## 3. AERODYNAMIC SYMBOLS

$S$ ,	Area	$i_w$ ,	Angle of setting of wings (relative to thrust line)
$S_w$ ,	Area of wing	$i_s$ ,	Angle of stabilizer setting (relative to thrust line)
$G$ ,	Gap	$Q$ ,	Resultant moment
$b$ ,	Span	$\Omega$ ,	Resultant angular velocity
$c$ ,	Chord	$\rho \frac{Vl}{\mu}$ ,	Reynolds Number, where $l$ is a linear dimension (e.g., for a model airfoil 3 in. chord, 100 m.p.h. normal pressure at 15° C., the cor- responding number is 234,000; or for a model of 10 cm chord, 40 m.p.s. the corresponding number is 274,000)
$\frac{b^2}{S}$ ,	Aspect ratio	$C_p$ ,	Center-of-pressure coefficient (ratio of distance of c.p. from leading edge to chord length)
$V$ ,	True air speed	$\alpha$ ,	Angle of attack
$q$ ,	Dynamic pressure = $\frac{1}{2}\rho V^2$	$\epsilon$ ,	Angle of downwash
$L$ ,	Lift, absolute coefficient $C_L = \frac{L}{qS}$	$\alpha_o$ ,	Angle of attack, infinite aspect ratio
$D$ ,	Drag, absolute coefficient $C_D = \frac{D}{qS}$	$\alpha_i$ ,	Angle of attack, induced
$D_o$ ,	Profile drag, absolute coefficient $C_{D_o} = \frac{D_o}{qS}$	$\alpha_a$ ,	Angle of attack, absolute (measured from zero- lift position)
$D_i$ ,	Induced drag, absolute coefficient $C_{D_i} = \frac{D_i}{qS}$	$\gamma$ ,	Flight-path angle
$D_p$ ,	Parasite drag, absolute coefficient $C_{D_p} = \frac{D_p}{qS}$		
$C$ ,	Cross-wind force, absolute coefficient $C_C = \frac{C}{qS}$		
$R$ ,	Resultant force		



---

---

**REPORT No. 590**

---

**PRESSURE-DISTRIBUTION MEASUREMENTS  
ON AN O-2H AIRPLANE IN FLIGHT**

**By H. A. PEARSON  
Langley Memorial Aeronautical Laboratory**

---

---

1

## NATIONAL ADVISORY COMMITTEE FOR AERONAUTICS

HEADQUARTERS, NAVY BUILDING, WASHINGTON, D. C.

LABORATORIES, LANGLEY FIELD, VA.

Created by act of Congress approved March 3, 1915, for the supervision and direction of the scientific study of the problems of flight. Its membership was increased to 15 by act approved March 2, 1929. The members are appointed by the President, and serve as such without compensation.

JOSEPH S. AMES, Ph. D., *Chairman*,  
President, Johns Hopkins University, Baltimore, Md.

DAVID W. TAYLOR, D. Eng., *Vice Chairman*,  
Washington, D. C.

CHARLES G. ABBOT, Sc. D.,  
Secretary, Smithsonian Institution.

LYMAN J. BRIGGS, Ph. D.,  
Director, National Bureau of Standards.

BENJAMIN D. FOULLOIS, Major General, United States Army,  
Chief of Air Corps, War Department.

WILLIS RAY GREGG, B. A.,  
Chief, United States Weather Bureau.

HARRY F. GUGGENHEIM, M. A.,  
Port Washington, Long Island, N. Y.

ERNEST J. KING, Rear Admiral, United States Navy,  
Chief, Bureau of Aeronautics, Navy Department.

CHARLES A. LINDBERGH, LL. D.,  
New York City.

WILLIAM P. MACCRACKEN, Jr., Ph. B.,  
Washington, D. C.

AUGUSTINE W. ROBINS, Brig. Gen., United States Army,  
Chief, Matériel Division, Air Corps, Wright Field, Dayton,  
Ohio.

EUGENE L. VIDAL, C. E.,  
Director of Air Commerce, Department of Commerce.

EDWARD P. WARNER, M. S.,  
Editor of Aviation, New York City.

R. D. WEYERBACHER, Commander, United States Navy,  
Bureau of Aeronautics, Navy Department.

ORVILLE WRIGHT, Sc. D.,  
Dayton, Ohio.

---

GEORGE W. LEWIS, *Director of Aeronautical Research*

JOHN F. VICTORY, *Secretary*

HENRY J. E. REID, *Engineer in Charge, Langley Memorial Aeronautical Laboratory, Langley Field, Va.*

JOHN J. IDE, *Technical Assistant in Europe, Paris, France*

---

### TECHNICAL COMMITTEES

AERODYNAMICS  
POWER PLANTS FOR AIRCRAFT  
AIRCRAFT STRUCTURES AND MATERIALS

AIRCRAFT ACCIDENTS  
INVENTIONS AND DESIGNS

*Coordination of Research Needs of Military and Civil Aviation*

*Preparation of Research Programs*

*Allocation of Problems*

*Prevention of Duplication*

*Consideration of Inventions*

### LANGLEY MEMORIAL AERONAUTICAL LABORATORY

LANGLEY FIELD, VA.

Unified conduct, for all agencies, of  
scientific research on the fundamental  
problems of flight.

### OFFICE OF AERONAUTICAL INTELLIGENCE

WASHINGTON, D. C.

Collection, classification, compilation,  
and dissemination of scientific and tech-  
nical information on aeronautics.



## REPORT No. 590

### PRESSURE-DISTRIBUTION MEASUREMENTS ON AN O-2H AIRPLANE IN FLIGHT

By H. A. PEARSON

#### SUMMARY

*Results are given of pressure-distribution measurements made over two different horizontal tail surfaces and the right wing cellule, including the slipstream area, of an observation-type biplane. Measurements were also taken of air speed, control-surface positions, control-stick forces, angular velocities, and accelerations during various abrupt maneuvers. These maneuvers consisted of push-downs and pull-ups from level flight, dive pull-outs, and aileron rolls with various thrust conditions.*

*The results from the pressure-distribution measurements over the wing cellule are given on charts showing the variation of individual rib coefficients with wing coefficients; the data from the tail-surface pressure-distribution measurements are given mainly as total loads and moments. These data are supplemented by time histories of the measured quantities and isometric views of the rib pressure distributions occurring in abrupt maneuvers.*

*The results indicate that there is little if any dissymmetry of load on the tail due to slipstream rotation and that the up loads may be as much as the down loads. From the results of the wing investigation it was found that the relative efficiency of the wings depended upon the type of maneuver.*

#### INTRODUCTION

Following the completion of pressure-distribution tests made of a PW-9 pursuit airplane in 1928 (reference 1), similar tests of an observation biplane were requested

by the Army Air Corps. The original object of this request was to institute a program that would lead to information on an observation type of airplane corresponding to the information already obtained on the pursuit type. An O-2H airplane was made available. Pressure of other work at the N. A. C. A. laboratories, however, delayed work on the rather extensive installation of apparatus, and flight tests could not be started until 1932.

Although the O-2H airplane was by then an obsolescent type and although the results of other related research projects had led to an improved understanding of many questions concerning external loads and their distribution on airplane structures, it was decided to complete the tests of the O-2H because it was believed that they would constitute a useful set of data with which modern methods of computing loads and load distribution might be compared.

The results are presented in a two-part paper, the first part giving the results of tests made of two tail surfaces and the second the results of an investigation over the right wing cellule and slipstream area.

#### APPARATUS

**Airplane.**—The airplane used in these tests (figs. 1 and 2) was a standard Army O-2H observation airplane with the following modifications: (1) The fabric covering on the fuselage from just abaft the engine hood to

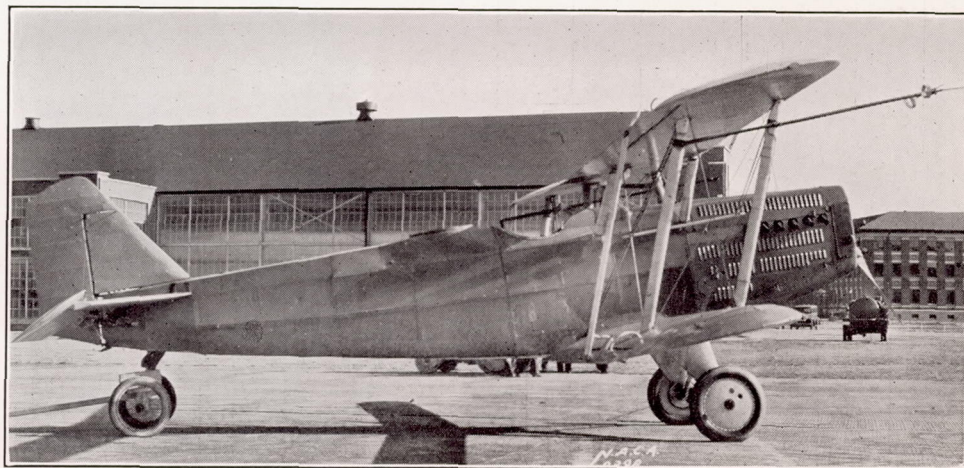


FIGURE 1.—The O-2H airplane.



the rear of the observer's cockpit was replaced by thin duralumin sheets that could easily be removed;

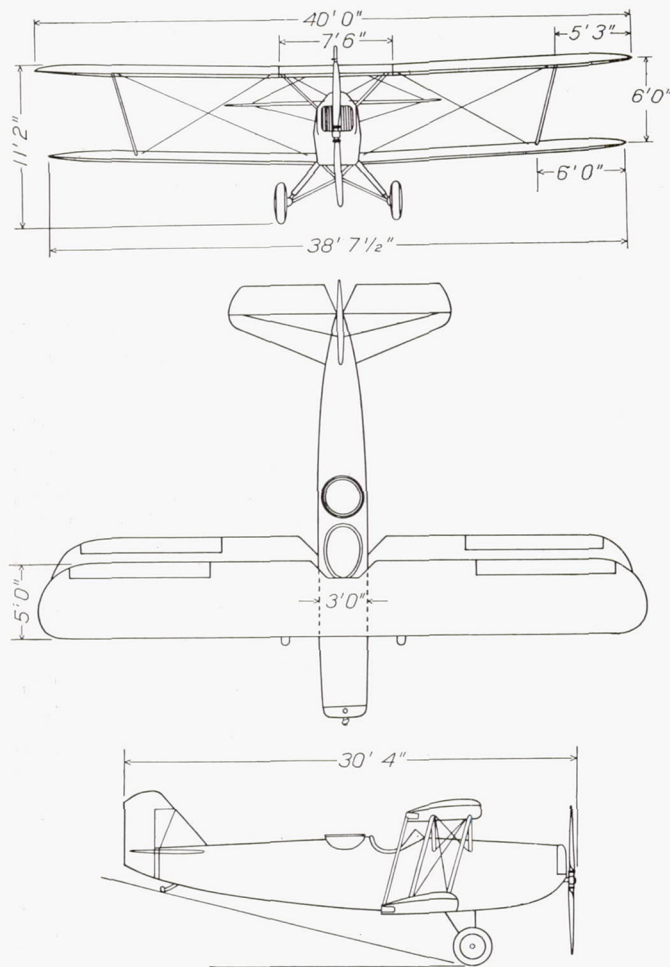


FIGURE 2.—Line drawing and dimensions of the O-2H airplane.

(2) the original 9.5-foot propeller was replaced by a 10.5-foot propeller; and (3) a boom carrying a swiv-

eling pitot head was attached to the interplane struts.

The two horizontal tail surfaces are shown in figures 3 (a) and 3 (b) and the wing surfaces are shown in figure 4. These figures give the location of the pressure points and other pertinent dimensions. Additional data

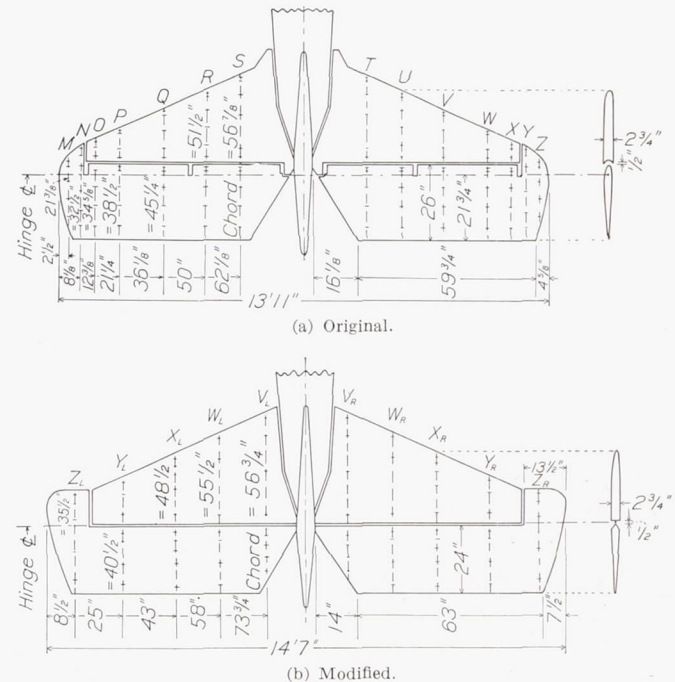


FIGURE 3.—Tail surfaces with pressure-rib and orifice locations.

concerning both the airplane and the various surfaces are given in table I.

**Pressure orifices and tubing.**—The orifice and tubing installation is much the same as that described in reference 1. For the tail-surface investigation the metal pressure tubes from both the elevator and the stabilizer were brought out in bundles near the fuselage (fig. 5), from which point they were connected by short lengths

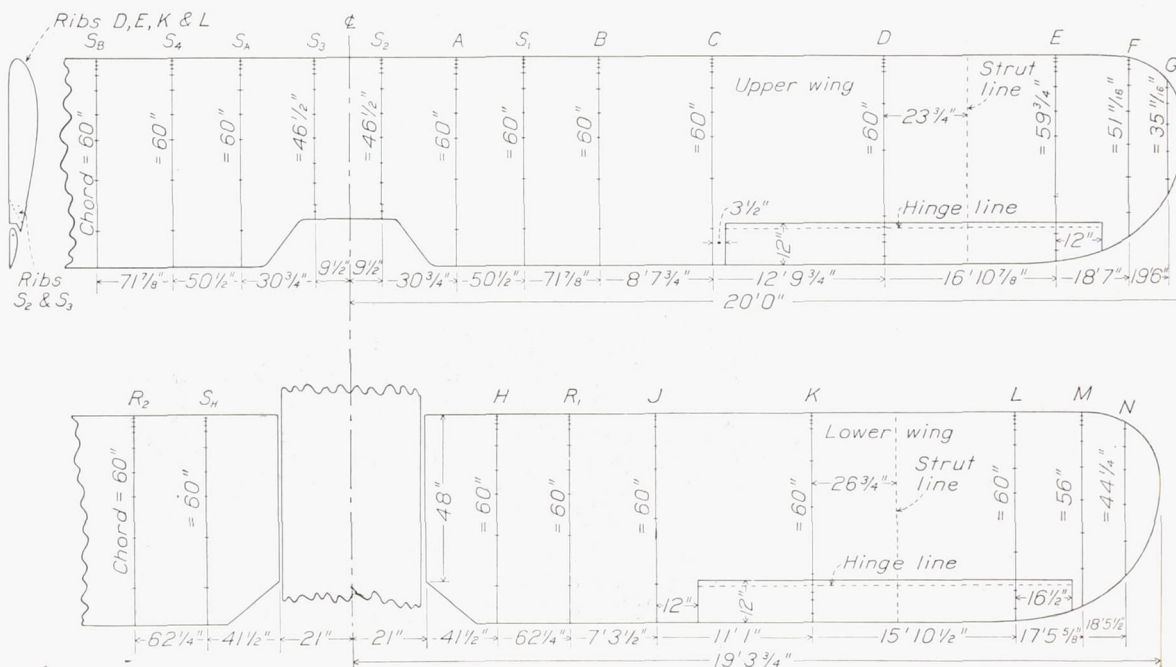


FIGURE 4.—Upper and lower wings of O-2H airplane with pressure-rib and orifice locations.



of rubber tubing to metal tubes leading directly to the manometers. For the wing investigation the tubing from the lower wing was carried through the wing root to the manometers and that from the upper wing was faired around the cabane struts and brought to the manometers. The tubing from the aileron ribs was grouped in small bundles, midway between the pressure ribs, and was connected by short pieces of rubber tubing to metal tubes within the wing.

**Instruments.**—Each pressure orifice was connected to a pressure cell on either of two N. A. C. A. type 60 multiple recording manometers located in the observer's cockpit midway between the upper and lower longerons. The pressure cells were similar to those of reference 1

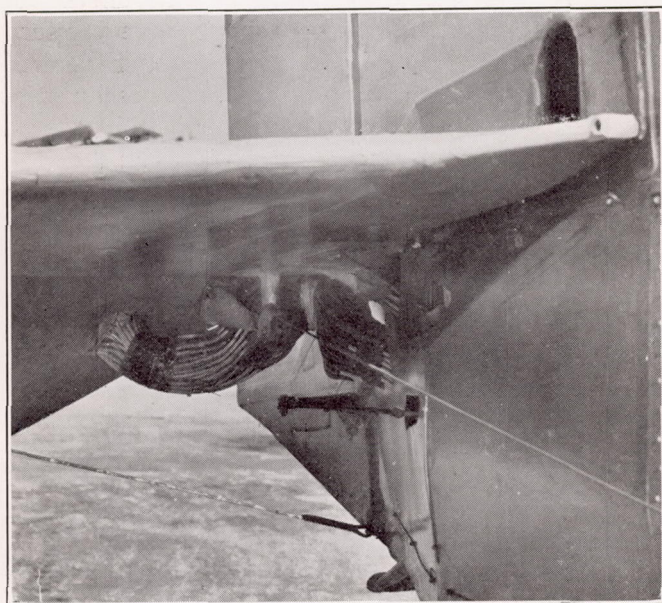


FIGURE 5.—Tail-surface tubing installation.

but were corrected for temperature effects by the method given in reference 2.

In the tail-surface investigation the load distribution occurring over each tail surface was measured during steady flight, dive pull-outs, and pull-ups from level flight. For the steady-flight condition the following standard N. A. C. A. photographically recording instruments were used: air-speed meter, control-position recorder, control-force recorder, inclinometer, and tachometer. For the pull-ups and pull-outs an accelerometer and a turnmeter, both located near the center of gravity of the airplane, were substituted for the inclinometer and tachometer used in the steady flights. All instruments were synchronized by an N. A. C. A. timer incorporated into their circuit.

In the wing-cellule and slipstream investigations the load distribution was measured in steady flight, push-downs and pull-ups from level flight, dive pull-outs, and aileron rolls. With the exception of an additional accelerometer mounted 18 inches in from the right wing

tip for the aileron rolls, the instruments were the same as used for the tail-surface investigation.

## I. PRESSURE-DISTRIBUTION TESTS OVER TWO SETS OF HORIZONTAL TAIL SURFACES

### METHOD

In the tests made of the modified tail (fig. 3 (b)), resultant pressures were recorded at 74 points. The remaining pressure cells were connected to wing ribs for the purpose of correlating the tail-surface and wing results. Subsequent tests showed this precaution to be unnecessary as the various stabilizer and elevator settings did not measurably affect the pressure distribution on the wing ribs. Consequently, in the series of tests of the original tail (fig. 3 (a)), the full 120 pressure cells were used on the tail alone.

**Steady dives.**—In order to obtain information on certain flap parameters, tail loads were measured during steady dives with the stabilizer in various settings. For the most part, the effect of the slipstream was minimized by running the tests near zero propeller thrust. Several tests were made, however, with the throttle fully closed and also with the throttle open to a position corresponding to what was considered to be a maximum safe engine speed. The method used to obtain zero thrust was to compute the  $V/nD$  for zero propeller thrust from an analysis of full-scale propeller tests. The pilot was then instructed to dive at a certain steady air speed and with a definite engine speed before taking records. Actually, this procedure required that the throttle be slightly opened.

In the tests of the modified tail, the stabilizer settings specified to the pilot were full nose heavy, full tail heavy, and trim.<sup>1</sup> Obviously, when trim was specified, several settings in the range of adjustment were possible depending upon the pilot's "feel" and the altitude at which he trimmed the airplane. This procedure led to complications in the analysis of the data owing to the number of variables involved. Consequently, in the tests of the original tail only three stabilizer settings were used: The two extreme settings and one midway between them.

With the exception noted, the test procedure for the two tail surfaces was the same and consisted of steady glides starting from 120 miles per hour and increasing by increments of roughly 10 miles per hour up to the maximum diving speed considered to be safe. The pressures measured at each point were the algebraic sum of those on the top and bottom of the airfoil surface (resultant pressures), no attempt being made to separate them. Simultaneously with these measurements, air-speed, control-force, control-position, inclinometer, and tachometer records were taken.

<sup>1</sup> "Stabilizer set tail heavy" as used here means that the stabilizer is set so as to make the tail seem heavy. From this definition the meaning of "trim" and "full nose heavy" settings is readily deduced.



The rib pressure-distribution curves for each tail rib were mechanically integrated to obtain the load and the moment of the load about the elevator-hinge center line. The rib loads and moments were then plotted against their span location and these curves, in turn, were integrated for the total load and moment of the tail. These results were then converted to tail load center of pressure with respect to the hinge line and finally to the moment exerted by the tail surfaces about the center of gravity of the airplane. A similar procedure was followed to obtain the load carried by the elevator and its hinge moment. The velocity used in all calculations for normal-force and hinge-moment coefficients was that given by a swiveling air-speed head located on a boom one wing chord length forward of the leading edge of the upper wing (fig. 1).

**Pull-ups.**—Pressure measurements were taken in abrupt pull-ups from steady level flight throughout the speed range with various stabilizer settings. Several graduated pull-ups from high-speed level flight and several pull-outs from shallow dives were also made. In these miscellaneous tests the stabilizer was set to trim.

In addition to the pressure measurements taken in the pull-up, records were also taken of the air speed, normal acceleration, angular velocity, control position, and control force. In most of the pull-up tests the results were computed from the records for only the time corresponding to the maximum down tail load. For the purpose of showing time histories, however, the results were in some cases computed for an interval that included the initial tail load and the subsequent maximum downward- and upward-acting tail loads.

The method by which total loads and moments were obtained from point pressures is the same as that previously explained.

#### PRECISION

A number of possible sources of error are present and may be listed as follows:

Individual pressure measurements may be incorrect because of—

- (a) Orifices not flush with surface.
- (b) Tube stopped or leaking.
- (c) Lag in tube and diaphragm.
- (d) Shrinkage of film.
- (e) Changed pressure-cell calibrations due to aging and temperature effects.
- (f) Personal errors in plotting and reading records.
- (g) Excessive width and haziness of pressure record line due to dust or oil on lens, small rapid pressure fluctuations, or vibration.

Rib loads and moments may be incorrect because of—

- (a) False individual pressures due to above errors.

- (b) Errors in plotting.
- (c) False fairing of curves due to insufficient points.
- (d) Integration errors.
- (e) Error introduced by neglecting the fore-shortening of the chord line with a control displacement. The resultant pressure at each point was, in all cases, plotted normal to the original chord line.

Sufficient checking was done to insure that errors in the individual pressures arising from sources (a) to (d) were negligible in these tests. The error due to source (e) was minimized by frequent calibrations and the use of temperature-compensated pressure cells. Errors due to (f) were practically eliminated by checking at all phases of the work. The largest source of error in the individual pressures is due to the haziness and width of the lines on the pressure records. Generally, the records taken in the dives were better in this respect than those in the pull-ups; also, those farther out on the tail were better than the ones close to the fuselage. The widths of the record lines were in some cases, where the deflections were small, so large as to make it impossible to tell whether a small positive or negative pressure existed. From the foregoing, it is obviously impossible to express the accuracy of the individual pressure on a percentage basis, since it varies with the amount of the local pressure, location of the pressure point, and the type of maneuver. The estimated maximum absolute error in the individual pressures was no more than 3 pounds per square foot for the high-range cells, which, in general, were connected to orifices located near the leading edges and close to the hinge center line. The error in the low-range cells was estimated to be no more than 1 pound per square foot. The low-range cells were connected to orifices located near the middle of the stabilizer ribs and at the trailing edges of the elevator.

The errors in rib loads due to source (e) were small in the case of the dives since the elevator displacements rarely exceeded  $15^\circ$ . In the abrupt pull-ups, however, where the elevator may be deflected as much as  $30^\circ$ , the error in the total tail load may be as much as 7 percent. This error does not enter into the elevator loads or moments.

The principal source of error in the rib-load curves is known to be in the fairing of the curves. The magnitude of this error varied with the type of pressure distribution obtained. In the steady dives with the stabilizer in the full nose-heavy setting, the error in the tail load due to fairing is believed to be a minimum and that obtained with the stabilizer in the other extreme position a maximum. In the nose-heavy case the maximum error in the tail load at speeds above 150 miles per hour is probably no more than 25 pounds as compared with 60 pounds for the full tail-heavy position. The maximum down tail loads occurring in the pull-ups



and pull-outs are estimated to be correct to within 50 pounds.

The indicated air-speed measurements are believed to be correct to within  $1\frac{1}{2}$  miles per hour as shown by several flights over a measured course. The recorded accelerations are accurate to within  $0.2\ g$  and the control-force measurements correct to within 3 pounds. Angular displacements, as given by the control-position recorder, are correct to within  $\frac{1}{2}^\circ$  and  $2^\circ$  for the stabilizer and elevator, respectively, while angular velocities about the center of gravity were measured to within  $0.05$  radian per second. Although tachometer readings were taken in the dives, no estimate of their accuracy is needed since it was found that the erratic effect of the various degrees of thrust in the tail-surface pressure-distribution tests did not exceed the effect that might arise from other errors. Consequently, in the following discussion, no discrimination is made regarding the various thrust conditions.

#### RESULTS AND DISCUSSION

**Steady dives.**—The variation of the tail moment about the center of gravity with air speed is given in

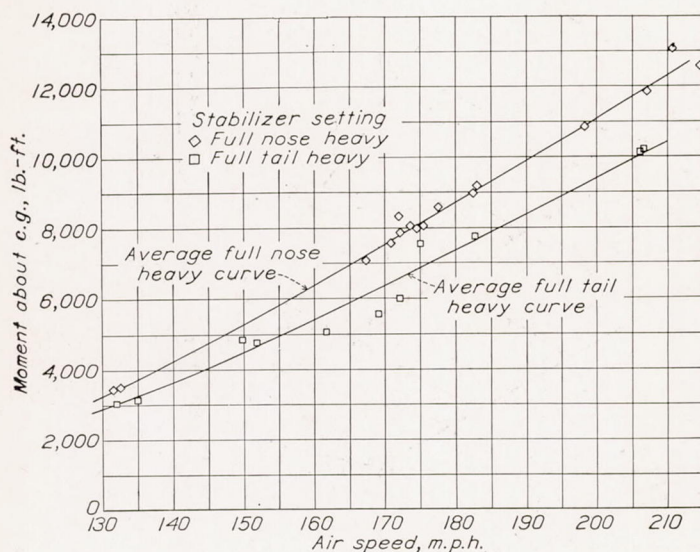


FIGURE 6.—Tail moment about airplane center of gravity (modified tail).

figures 6 and 7 for the modified and original tail surfaces, respectively. From these figures it appears that the moment furnished by the tail, at a given air speed, is considerably affected by the stabilizer setting. Since the tail surfaces provide a moment about the center of gravity of the airplane that balances the resultant moment due to all other parts, it would be expected that the moment furnished by the tail would be approximately constant. The tail-moment curves, however (figs. 6 and 7), indicate that, as the stabilizer moves toward the tail-heavy position, the moment becomes smaller and the scattering of the experimental points becomes greater.

Typical curves for the pressure distribution measured over the tail-surface ribs are given in figures 8 to 12. Figures 8 and 9 are for the modified tail surfaces and figures 10, 11, and 12 are for the original tail. The ordinates of these rib pressure-distribution curves are given in terms of the ratio  $p/q$  where  $p$  is the local pressure difference and  $q$  is the dynamic pressure measured at the air-speed head. A comparison of the results for identical stabilizer settings either in figures 8 and 9 or in figures 10, 11, and 12 shows an increase in peak pressure at the stabilizer leading edge with an increase in air speed. Although this difference in peak pressure is due to the cumulative effect of several factors, such as possible changes in interference, downwash, and elevator angle, it is thought that the greater

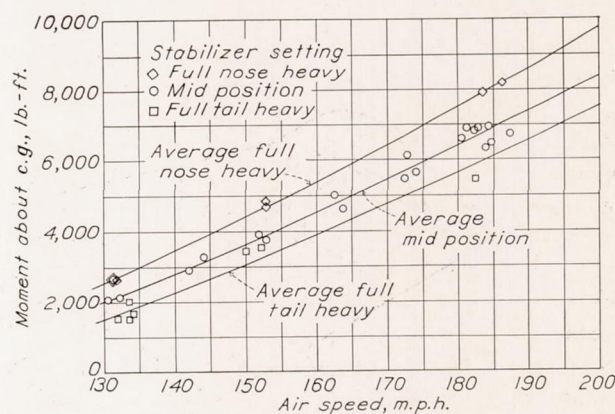


FIGURE 7.—Tail moment about airplane center of gravity (original tail).

structural deflection which occurs at the highest speed would account for a good portion of the variation with air speed. Static tests with a loading corresponding to that of the full tail-heavy setting for the modified tail indicated that at 170 miles per hour the change in stabilizer angle due to this structural deflection was approximately  $1^\circ$ .

The pressure distributions shown over ribs  $Z_R$  and  $Z_L$  (figs. 8 and 9) seem to indicate that with small elevator deflection the balance portion is of little value in reducing the stick loads. A similar conclusion is inferred in reference 3, in which calculated balance coefficients obtained by the usual methods were not verified by the pilots' observations. The rib-pressure diagrams for the original tail (figs. 10, 11, and 12) show that in the dives the peak pressure on the elevator occurs nearer to the hinge line than to the leading edge; however, in the dives the elevator leading edge seldom projects either above or below the stabilizer surfaces.

The form of the rib-pressure diagrams for the full tail-heavy setting explains the tendency to the wide scattering of the experimental points given in figures 6 and 7 for this setting. Figures 8 to 12 show that for the tail-heavy setting the resultant tail load is the difference between upward- and downward-acting loads, either one of which is larger than the resultant.



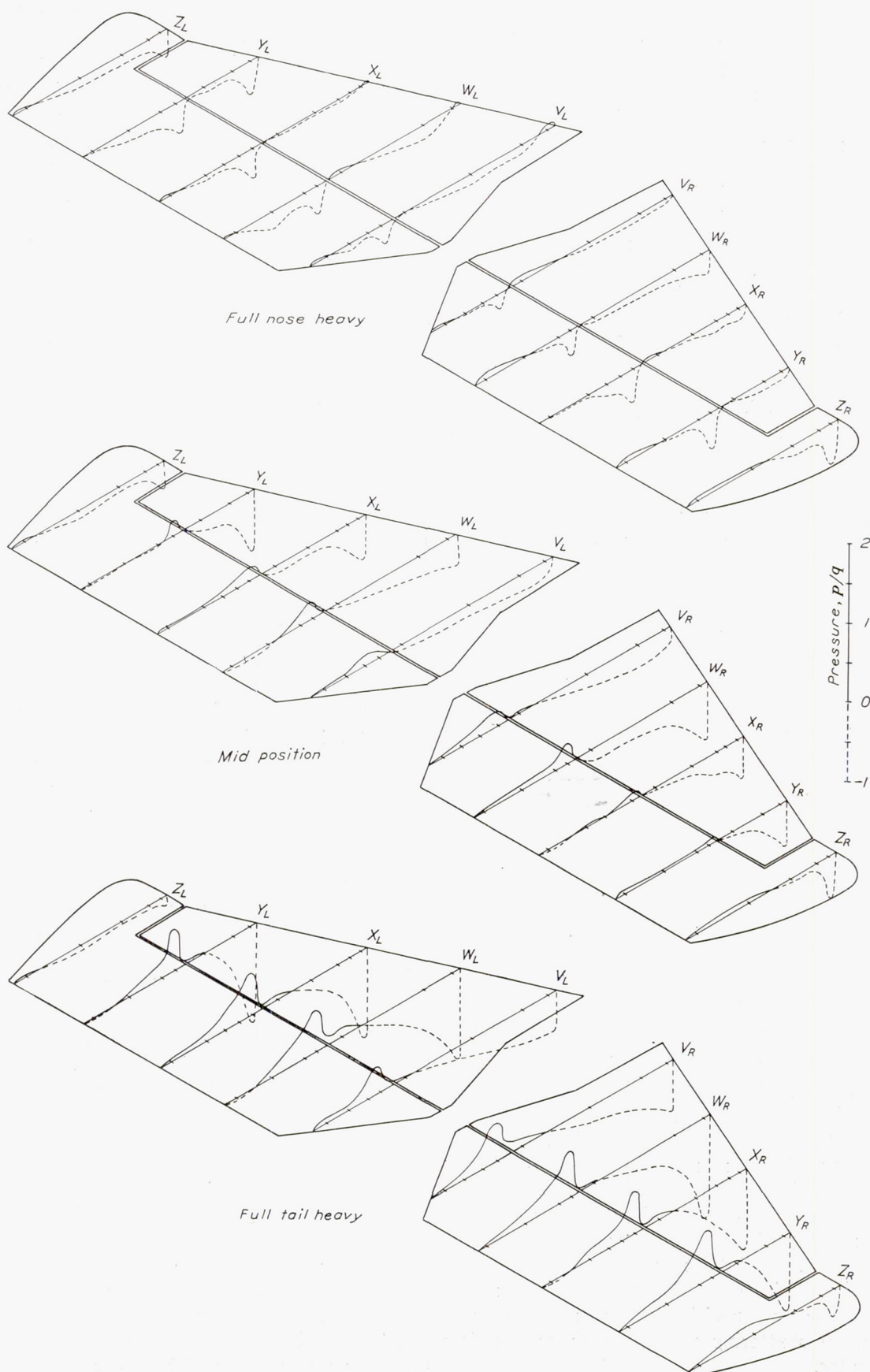


FIGURE 8.—Distribution of resultant pressures on modified tail surfaces for different stabilizer settings at 130 miles per hour.



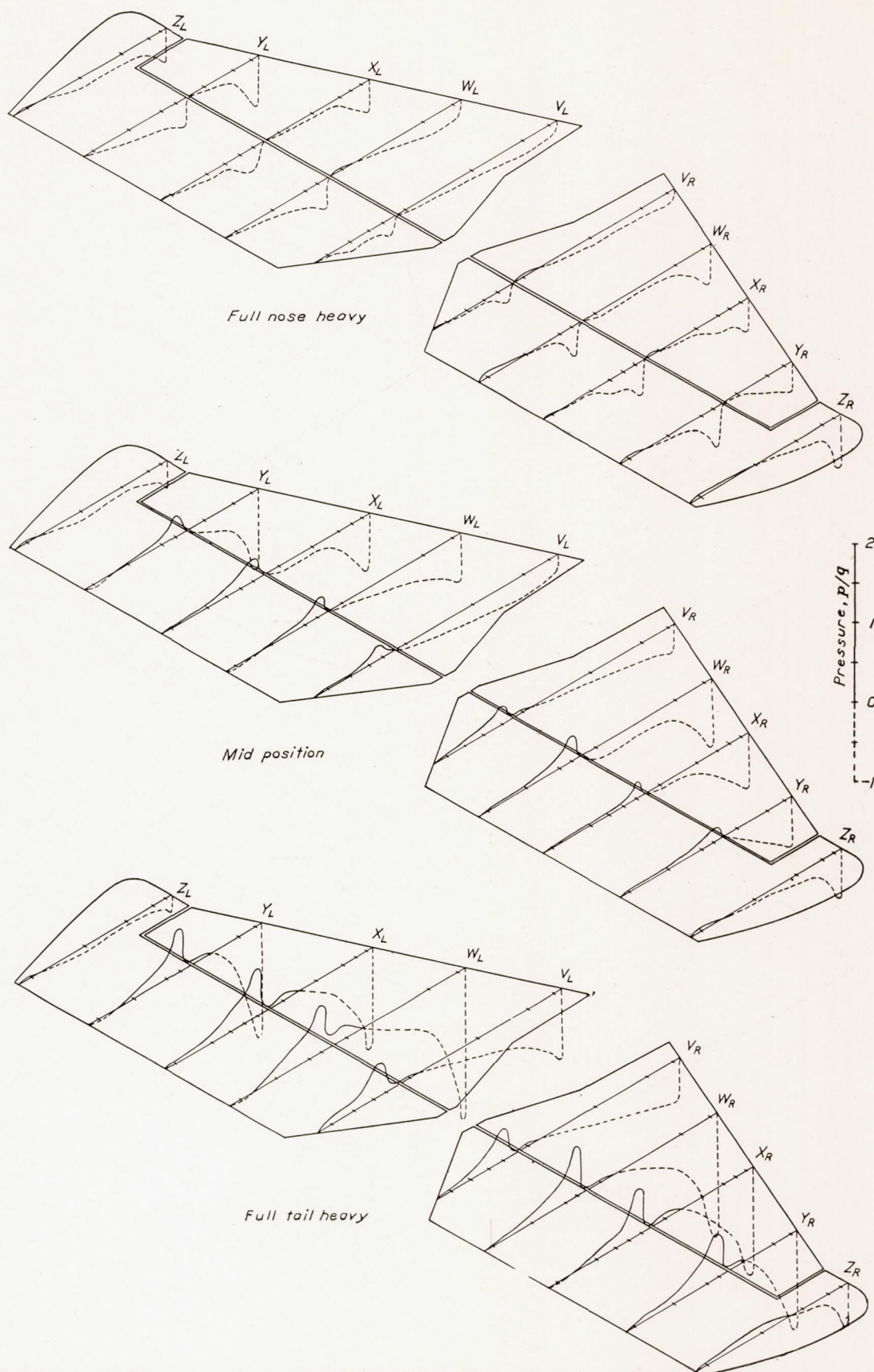


FIGURE 9.—Distribution of resultant pressures on modified tail surfaces for different stabilizer settings at 170 miles per hour.



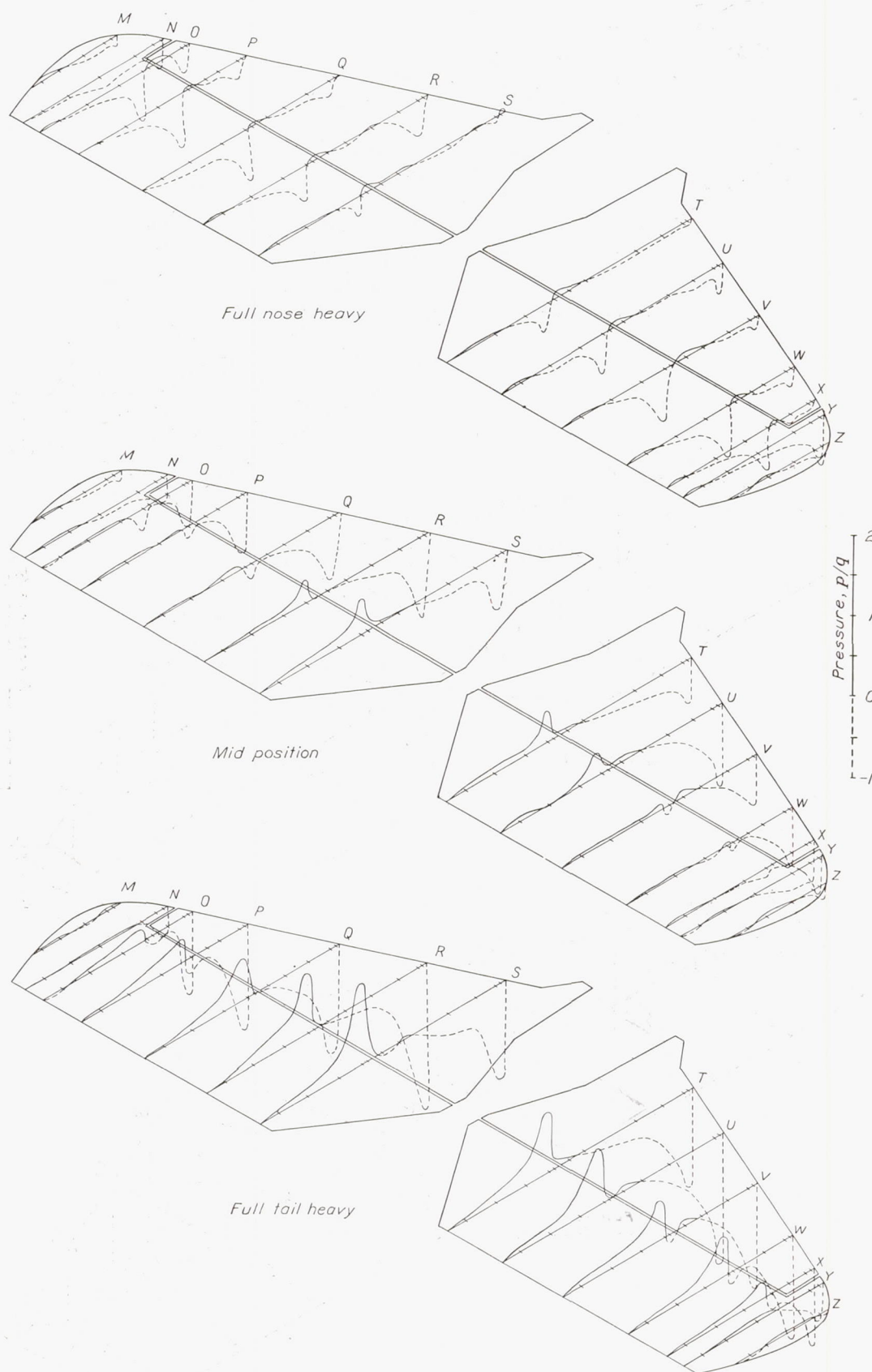


FIGURE 10.—Distribution of resultant pressures on original tail surfaces for different stabilizer settings at 130 miles per hour.



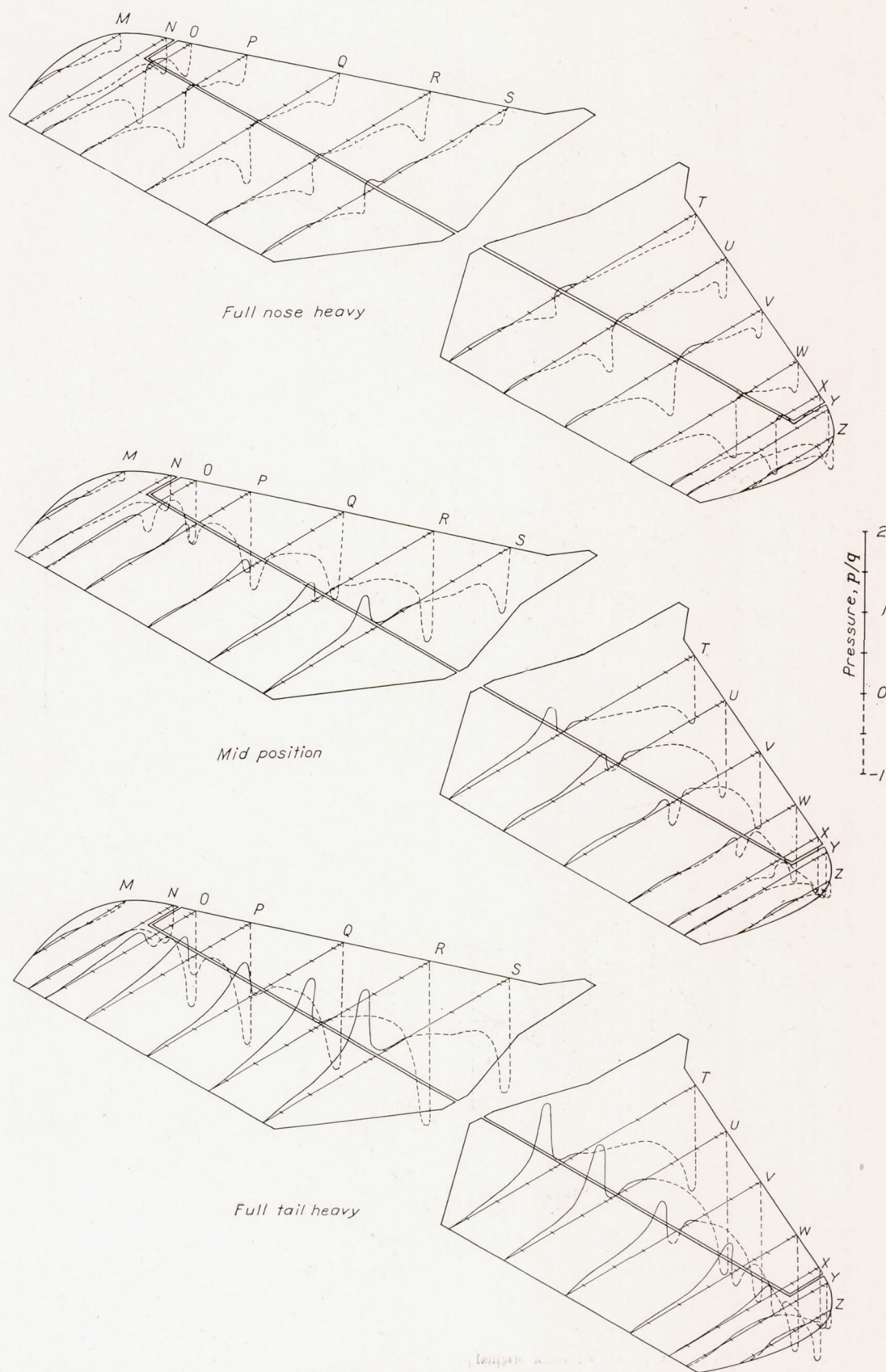


FIGURE 11.—Distribution of resultant pressures on original tail surfaces for different stabilizer settings at 150 miles per hour.



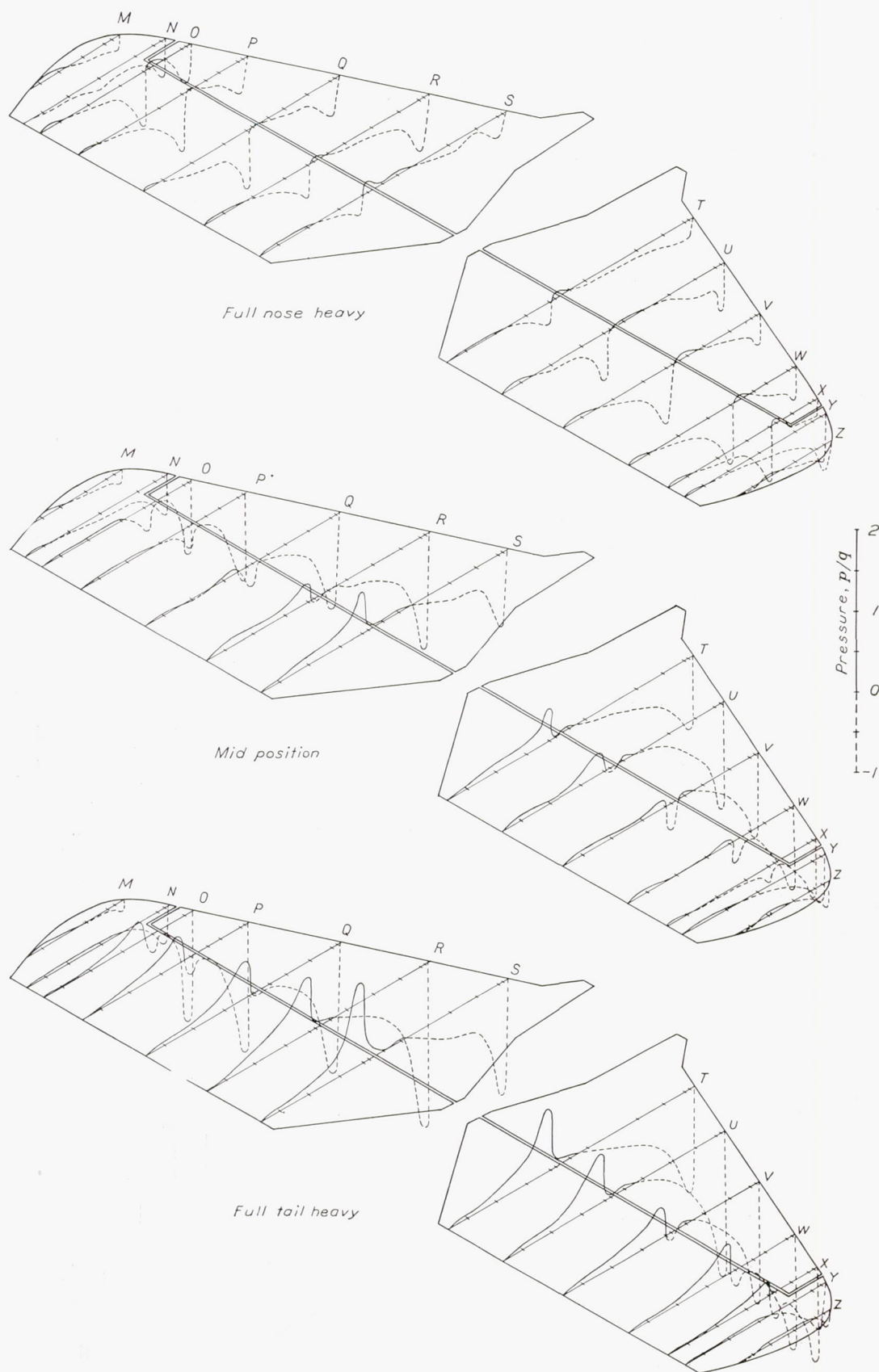


FIGURE 12.—Distribution of resultant pressures on original tail surfaces for different stabilizer settings at 180 miles per hour.



Because of this condition, small inaccuracies in fairing may lead to considerable dispersion in the final results. Aside from the inaccuracy due to fairing, the individual rib loads, and consequently the tail loads, are likely to be low for the full tail-heavy setting owing to the fact that the large down pressures at the leading edge could not be measured. Since the rib-pressure curves for the stabilizer set full nose heavy are not subject to these sources of discrepancy, it is felt that the moment curves for this setting (figs. 6 and 7) are more indicative of the true moment than any of the others.

In order to gain an idea as to how the experimental moment curves for the nose-heavy settings compare with the computed ones, several curves, representing varying degrees of refinement, are given (fig. 13). Curve A is for the case when only the moments of the two wings about their quarter-chord points are taken into account; in curves B the moment about the airplane center of gravity has been computed for the case when the additional moments due to the lift and drag vectors are also included. These vectors were assumed to act at the wing quarter-chord points and their magnitudes were determined from the relative lift distribution between the wings, which was determined in the wing investigation. As the airplane centers of gravity were different (table I) for the two tail-surface investigations, two separate curves were required.

Curves C also include the probable effect of the fuselage on the moment about the center of gravity, assuming that the fuselage exerts a constant moment given by

$$M_f = C_{mf} q A_f c_f$$

where  $C_{mf}$  is the moment coefficient, 0.01.

$A_f$ , horizontal projected area, 65 square feet.

$c_f$ , fuselage length, 27 feet.

The value of the moment coefficient defined by the foregoing equation was taken to be 0.01 after an analysis of the data contained in reference 4. The final comparisons (curves C and D) could no doubt be improved if it were possible to include the effect of the landing gear and tail surfaces. The moments that they introduced were, however, of opposite sign and tended to cancel.

The span load distribution across the tail for the foregoing rib pressure-distribution plots is given in figure 14. These curves show irregularities that are more or less to be expected owing to the irregular nature of the flow over the tail surfaces and to the comparatively small loads measured in the steady dives. An analysis of the data indicated that, in spite of the irregularity of the loading, the average difference in load between the two halves of the tail was of the order of 3 percent and 5 percent of the total load for the original and modified tail, respectively. Inasmuch as the sides that carried the most load varied between the two tail surfaces, it must be concluded that the difference in load is due to slight differences in rigging rather than to a slipstream effect.

In these tests the elevator moments about the hinge axis were obtained from both the pressure distribution and the control-force-recorder measurements; the results are compared in figure 15 for the original tail. In order to make this comparison between the two hinge moments, however, it was necessary to correct the measurements given by the control-force recorder for the moment exerted by the elevator (because of its unbalanced weight) about the hinge line and for the moment exerted by the unbalanced weight in the stick about its pivot point. Although the magnitude of the friction moment was known, it was impossible to correct for it in the steady dives because its direction was unknown. Even with these corrections the moments given by the control-force recorder were found to be more consistent than those given by pressure-distribution measurements and hence were used for computing hinge-moment coefficients.

The variation of the hinge-moment coefficient with elevator angle is given in figures 16 and 17 for the

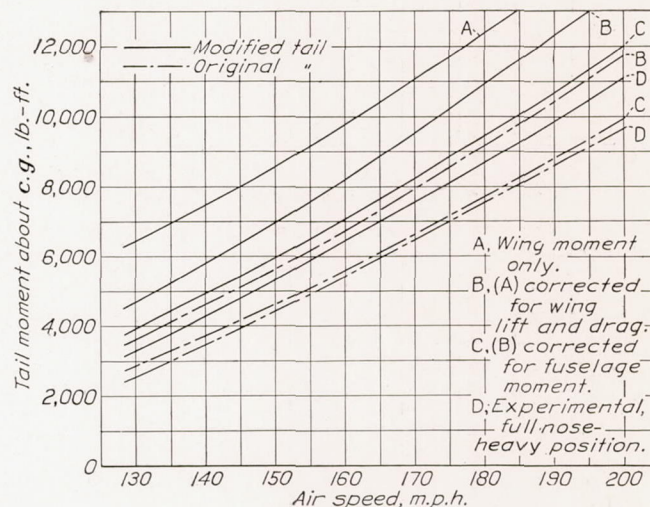


FIGURE 13.—Computed and experimental tail moments about the center of gravity

modified and original tail surfaces, respectively. These coefficients have been computed from the relation

$$C_{he} = \frac{M_e}{q S_e c_e}$$

where  $M_e$  is the elevator hinge moment given by the control-force recorder.

$c_e$ , the average elevator chord obtained by dividing the elevator area behind the hinge line by the elevator span.

$S_e$ , the elevator area behind the hinge line.

Although the points for the modified tail (fig. 16) show a fairly close grouping to a common line, those for the original tail (fig. 17) indicate considerable dispersion. Even though the scattering of these points is fairly large, it can be seen that there is a tendency for the points to move upward as the tail normal-force coefficient increases negatively. This shift is in qualitative agreement with the theory for an airfoil with a flap.



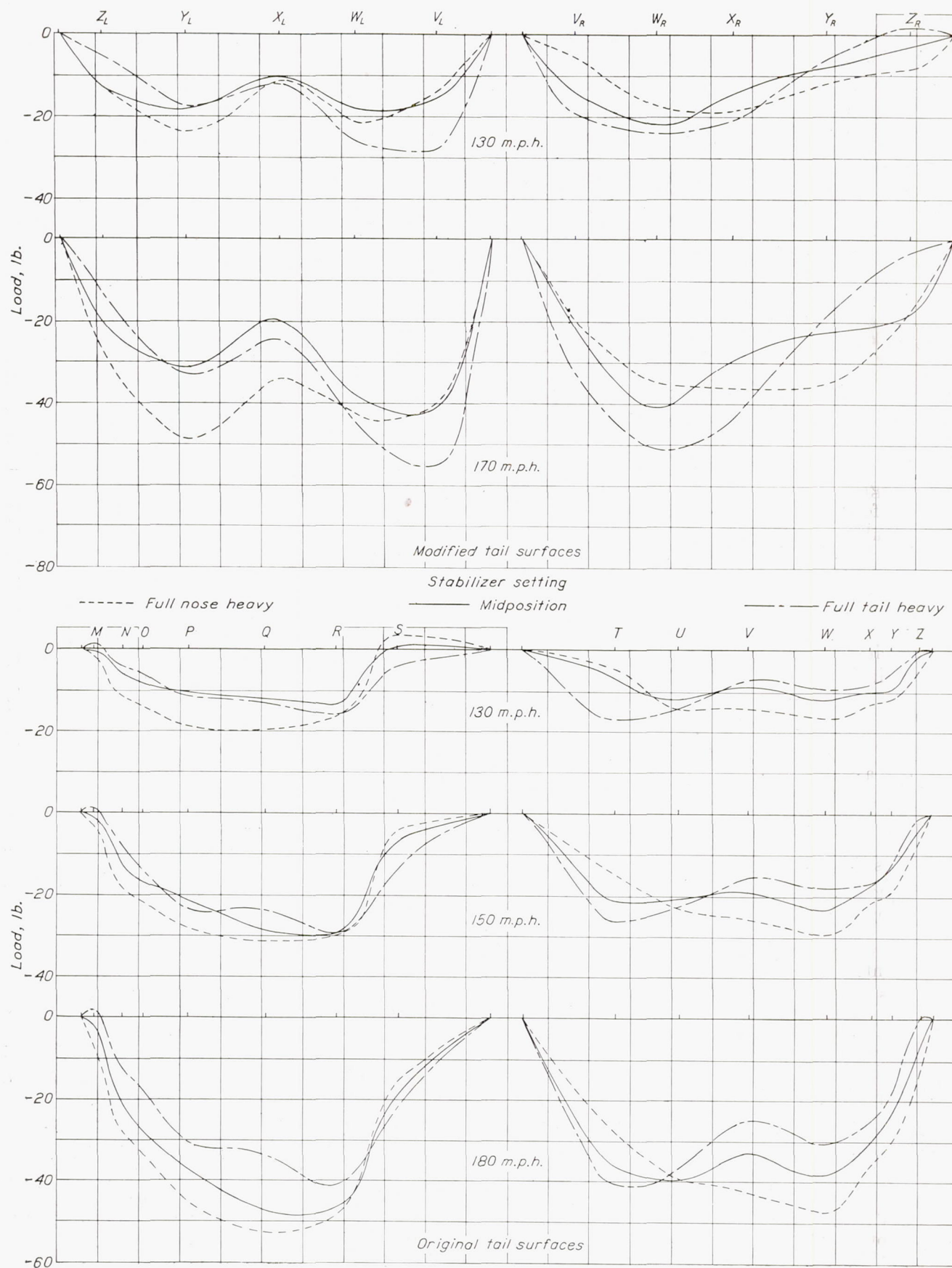


FIGURE 14.—Span load distribution in steady dives.



**Pull-ups.**—Typical results of the pull-up tests of the original tail are given in figures 18 to 24. Figures 18 and 19 are time histories of the measured quantities in abrupt pull-ups from level flight at various air speeds with the initial stabilizer settings full nose heavy and full tail heavy, respectively. Figure 20 presents time histories of two fairly abrupt pull-outs from dives at approximately 170 miles per hour with the stabilizer trimmed.

The time histories shown in figures 18 and 19 indicate that the maximum down tail loads occurring in the abrupt pull-ups vary with stabilizer setting. At a given air speed the loads with the stabilizer in an initially

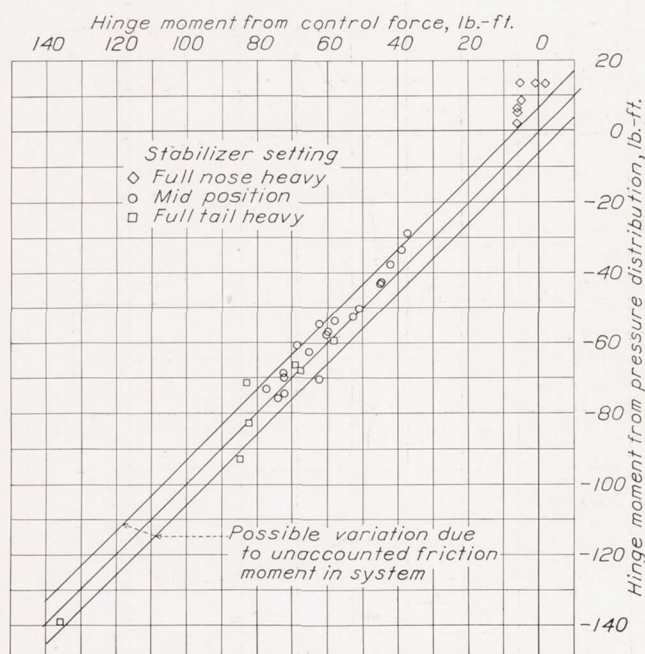


FIGURE 15.—Comparison of elevator hinge moments obtained from pressure-distribution measurements with those obtained from control-force measurements (original tail).

full tail heavy setting are greater than those when the stabilizer is in the other extreme position, but it should be noted that in the nose-heavy setting the total elevator displacements are less. Regardless of stabilizer setting, however, the tail load reaches a maximum with the maximum elevator displacement and before the airplane has had a chance to pitch. The load then quickly decreases and reaches a positive maximum as the airplane gains angular velocity. This positive maximum is generally less than the down load and occurs at about the same time as the maximum acceleration at the center of gravity. In the space of 1.0 second the tail has thus undergone two peak loadings of opposite sign.

The most interesting item occurring in figure 20 is a measured up load greater than the maximum down load. In this run (run 79) it may be observed that the acceleration mounted rapidly toward  $6g$ , where it was abruptly checked when the pilot returned the elevator to neutral. This condition probably occurs quite

frequently in airplanes performing acrobatics and the horizontal tail surfaces for such airplanes should consequently be designed to withstand the same load in both directions.

The evolution of the rib pressure distribution occurring in the abrupt pull-ups from level flight at approximately 115 miles per hour is shown in figures 21 and 22. These diagrams correspond to runs 67 and 70 of figures 18 and 19, respectively. Similarly, figure 23 shows the rib pressure distribution occurring in the dive pull-out represented by run 77 of figure 20. It can be seen from these diagrams that with the larger elevator displacements the horn balance performs its

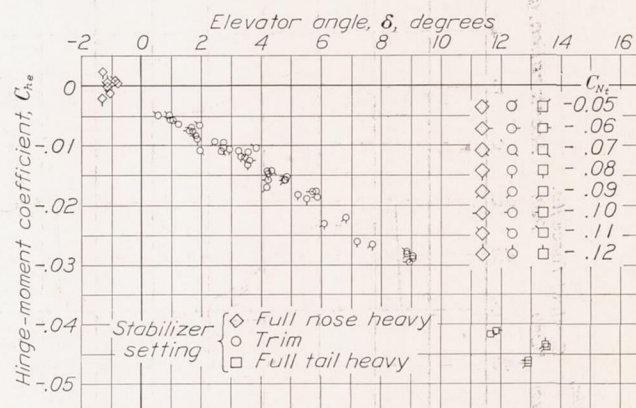


FIGURE 16.—Elevator hinge-moment coefficients with the modified tail.

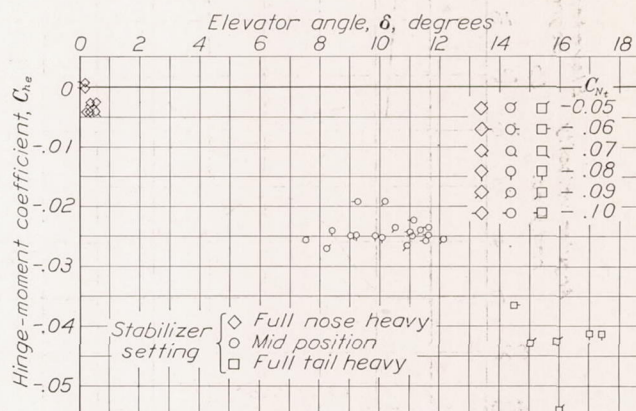


FIGURE 17.—Elevator hinge-moment coefficients with the original tail.

proper function. The Handley Page part of the balance, however, does not contribute so much toward balancing during the first phase of the pull-up as would be expected and during the latter phase it works against balance.

A typical variation of the change in the spanwise load distribution with time is given in figure 24 and corresponds to the results given in figure 22. The shape of the loading curve is more regular than in the steady dives mainly because the larger loads result in larger recorded deflections, which may be read with a greater percentage of accuracy. Another reason for the greater regularity may be that in the pull-up the tail surfaces tend to swing out of the relatively irregular slipstream area.



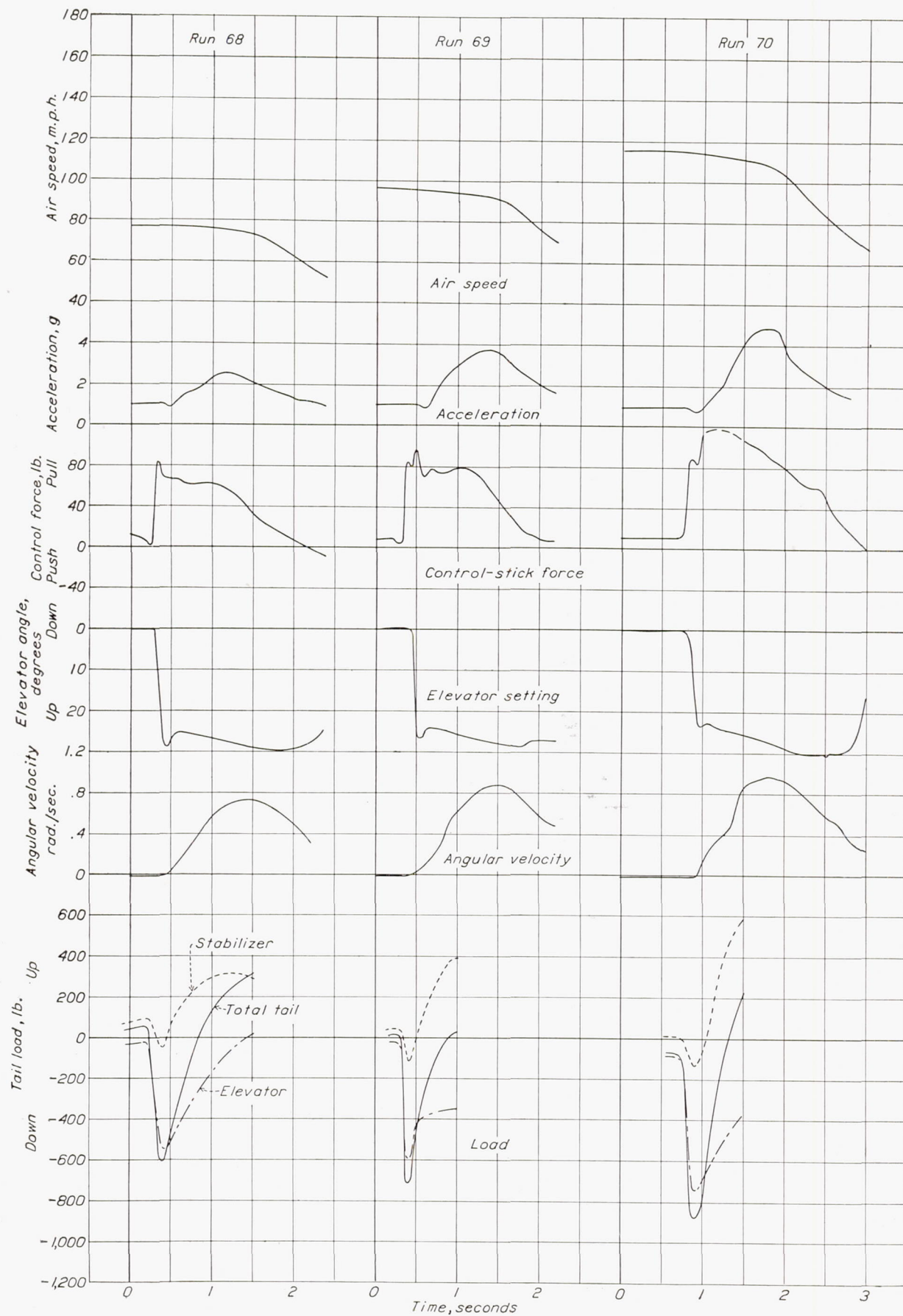


FIGURE 18.—Time history of pull-ups from level flight (stabilizer full nose heavy, original tail).



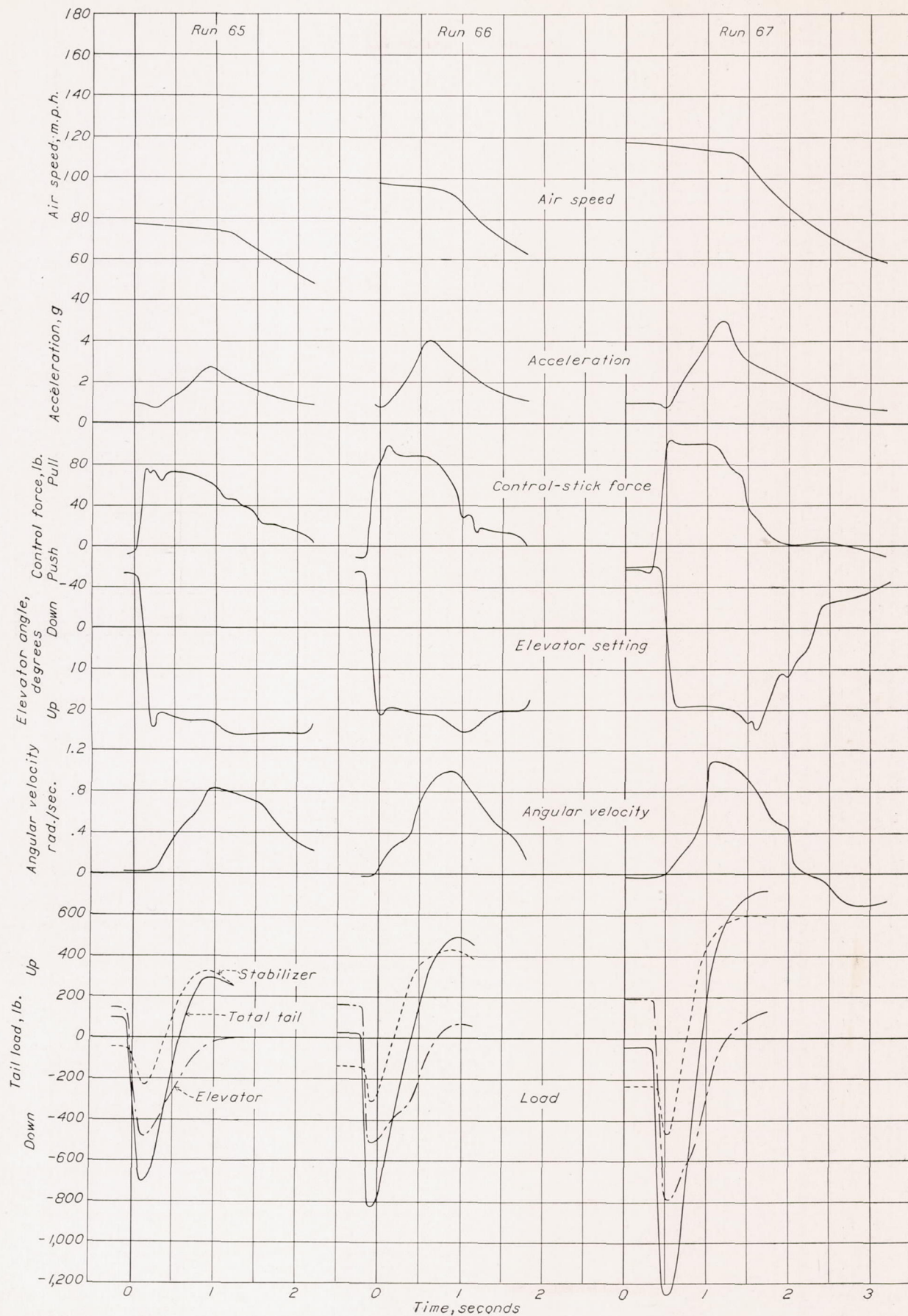


FIGURE 19.—Time history of pull-ups from level flight (stabilizer full tail heavy, original tail).



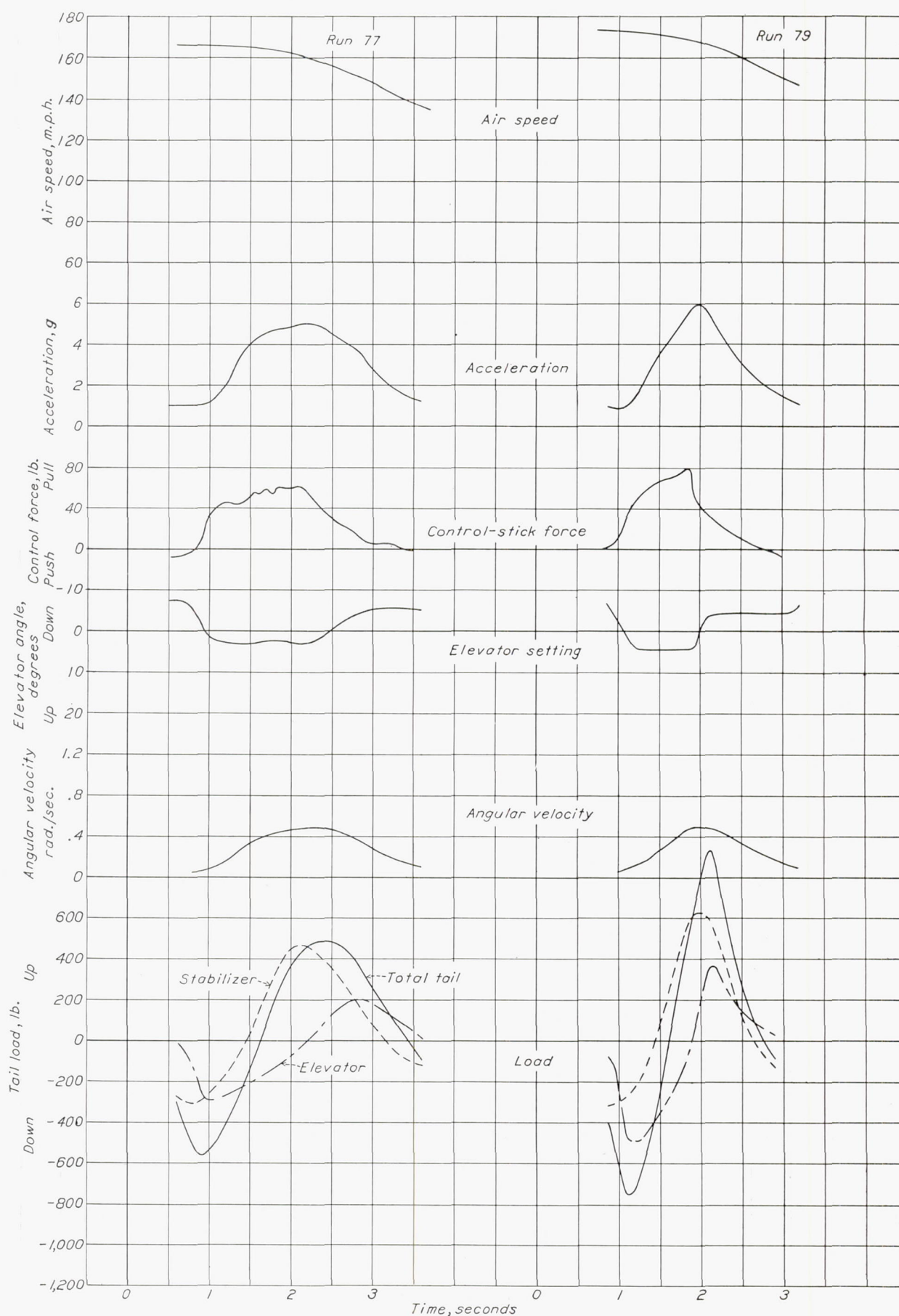


FIGURE 20.—Time history of pull-outs from dives (stabilizer set to trim, original tail).



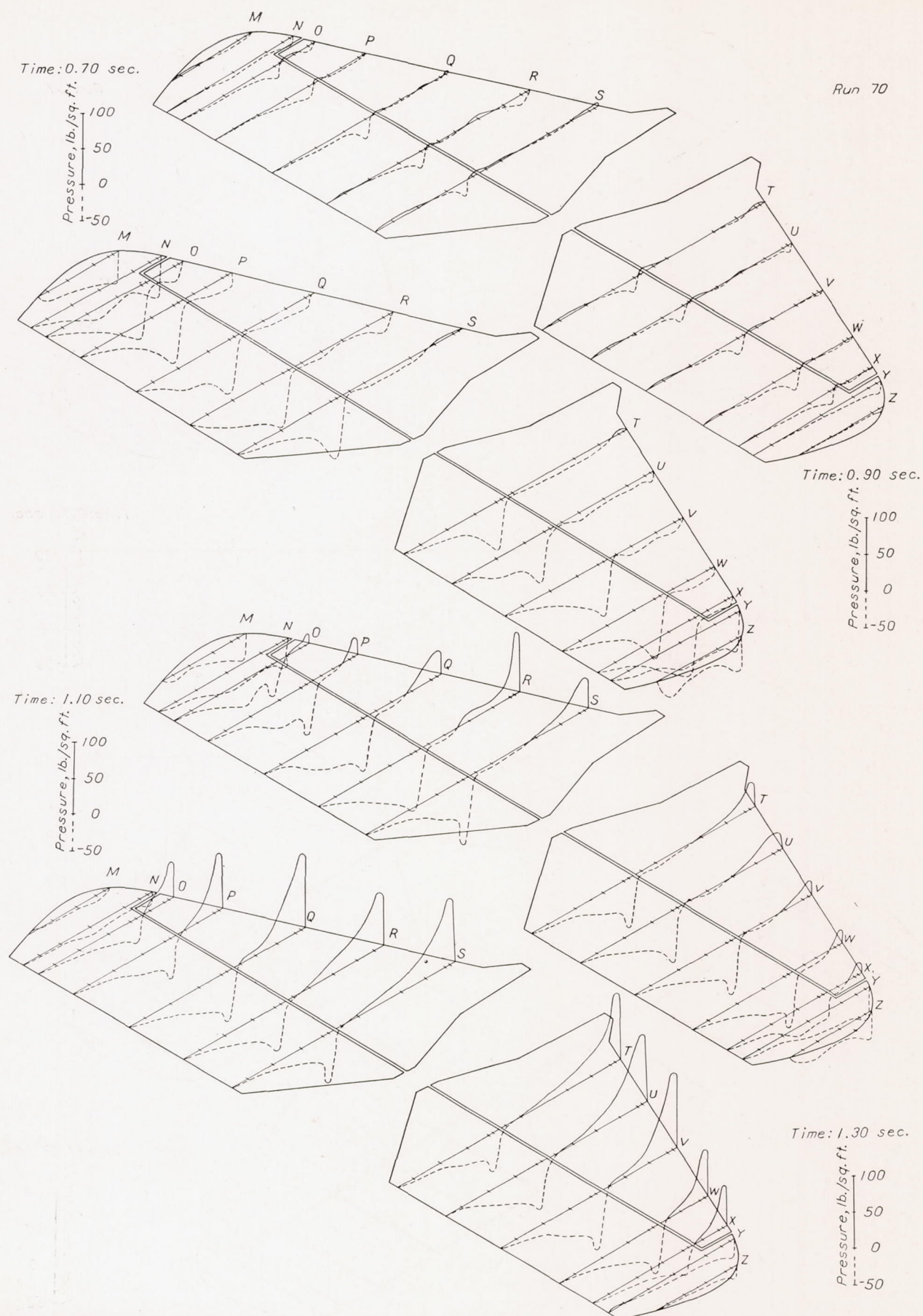


FIGURE 21.—Distribution of resultant pressures at various stages of a pull-up from level flight at 115 miles per hour (stabilizer full nose heavy).



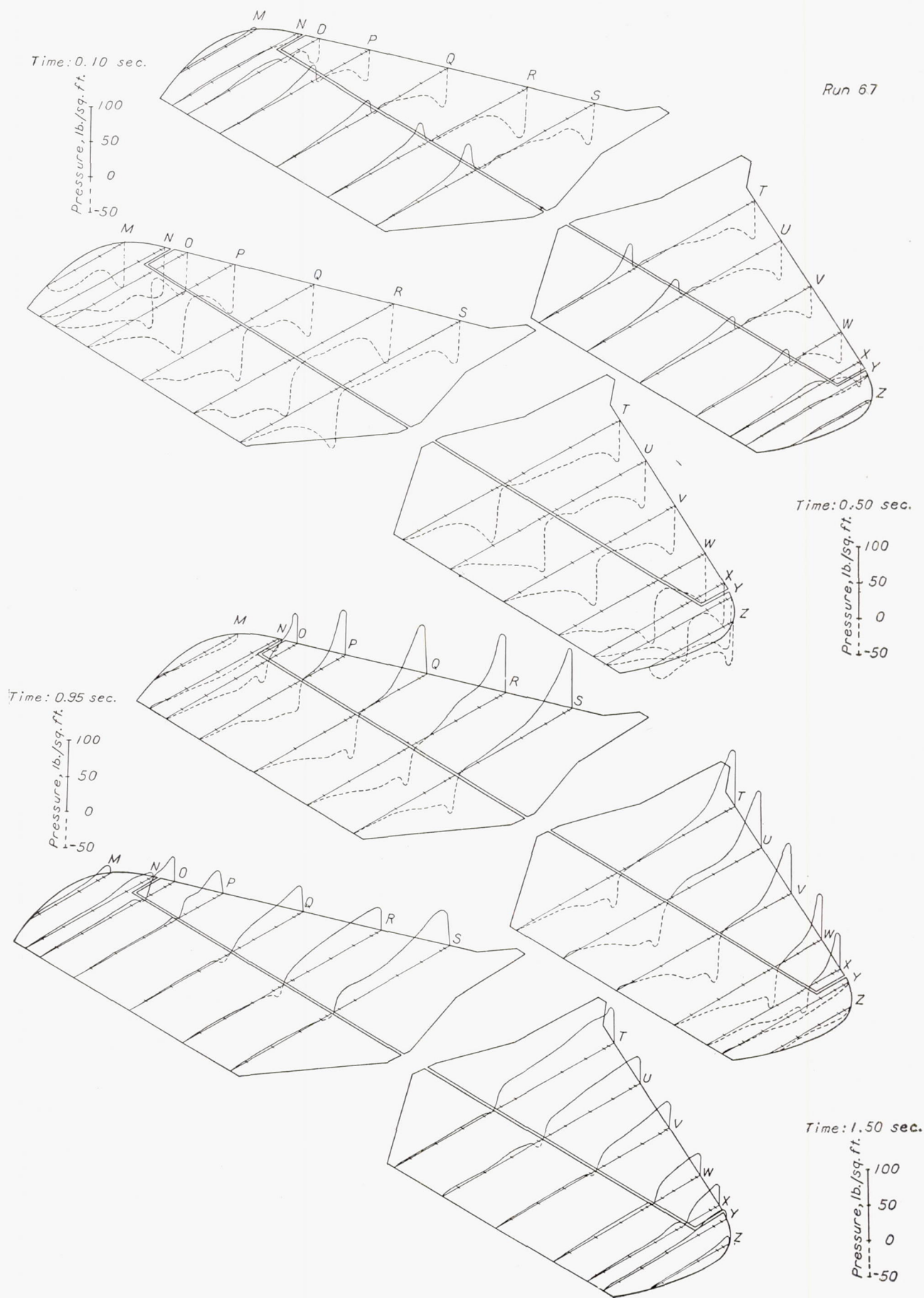


FIGURE 22.—Distribution of resultant pressures at various stages of a pull-up from level flight at 117 miles per hour (stabilizer full tail heavy).



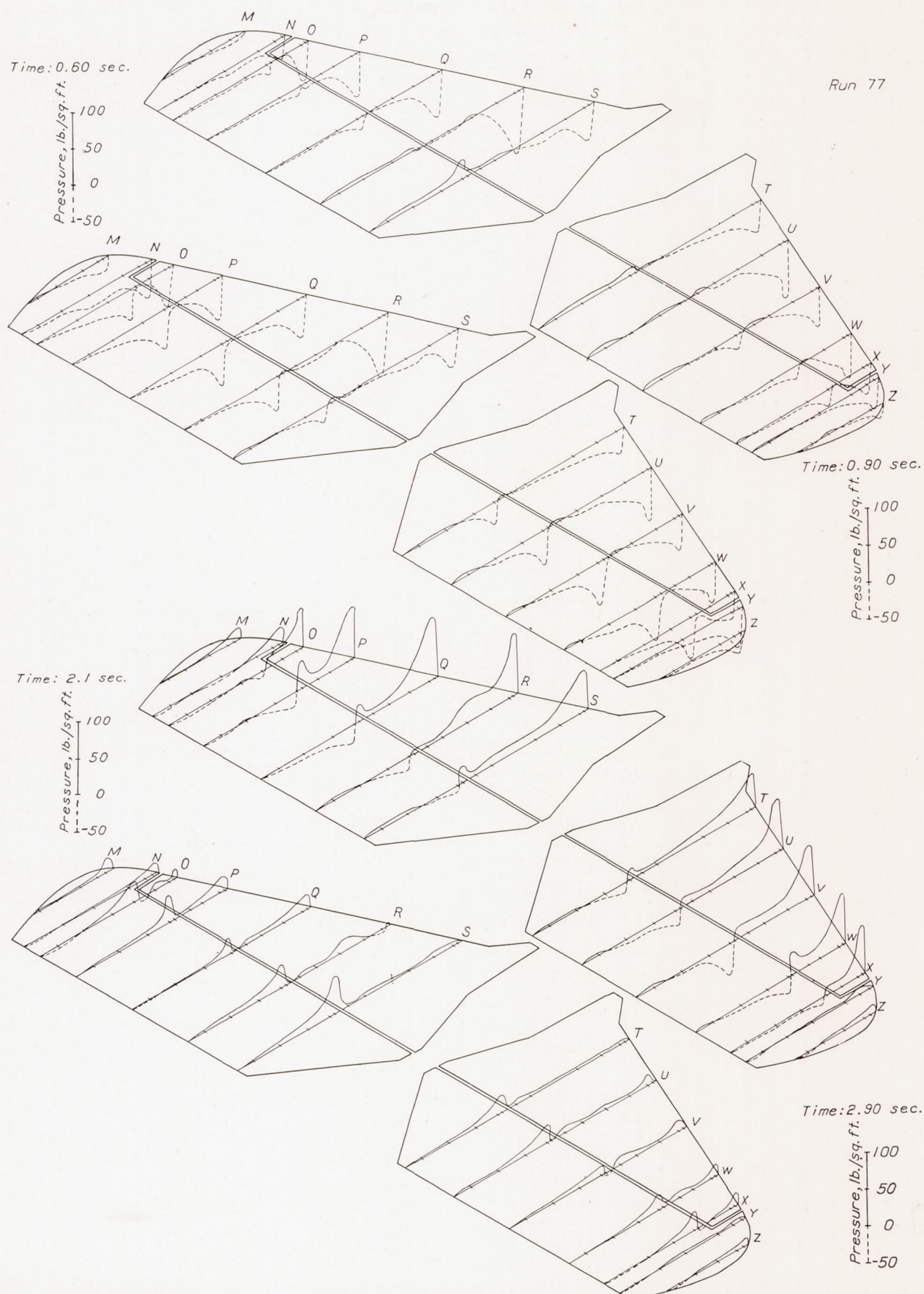


FIGURE 23.—Distribution of resultant pressures at various stages of a pull-out from a dive at 166 miles per hour (stabilizer set to trim).



Although the foregoing figures (figs. 18-24) have given results for the original tail, they also typify those obtained with the modified tail. In figures 25 and 26, however, over-all loads and coefficients are given for both tail surfaces. Figure 25 gives the variation with air speed of the maximum loads measured in abrupt pull-ups from level flight and figure 26 is a plot of the

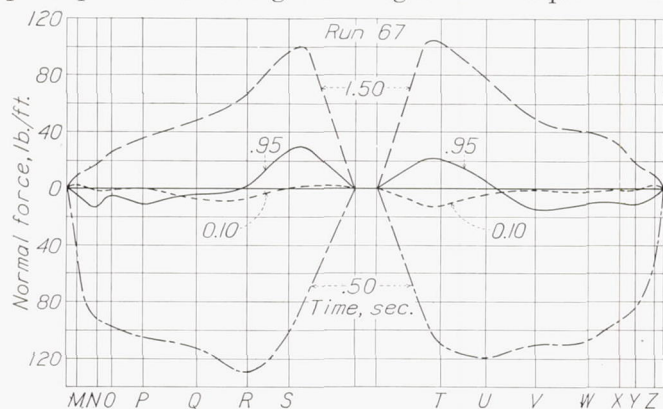


FIGURE 24.—Distribution of normal force along the span of the original tail during a pull-up from level flight at 117 miles per hour (stabilizer full tail heavy).

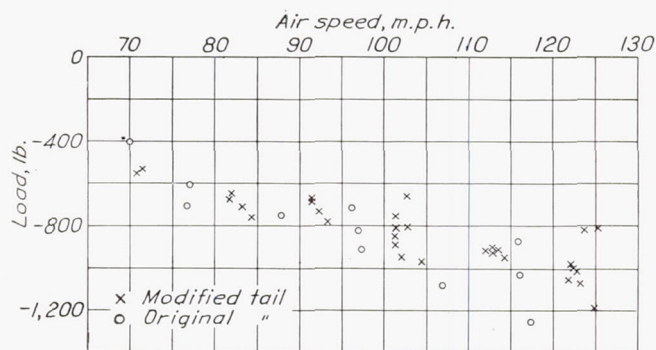


FIGURE 25.—Maximum down tail loads measured in abrupt pull-ups from level flight

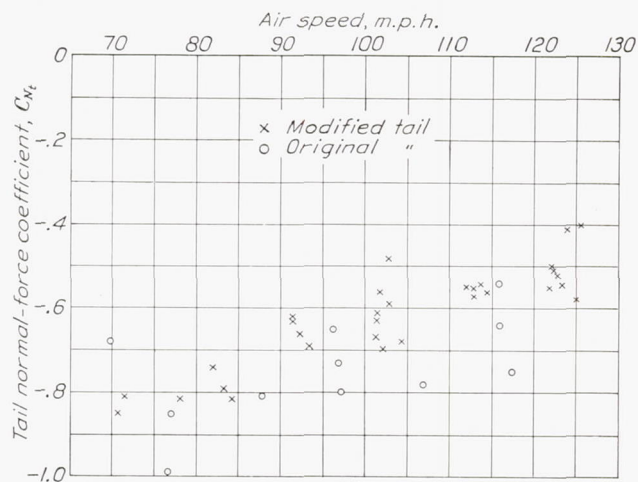


FIGURE 26.—Maximum values of the tail normal-force coefficient measured in abrupt pull-ups from level flight.

corresponding normal-force coefficients, computed from the relation

$$C_{N_t} = \frac{\text{tail load}}{q S}$$

where  $S$  is the actual tail area including the balances, in square feet. The maximum loads measured are of the

same order of magnitude, about 1,200 pounds, for both tail surfaces. For the original tail, however, the maximum unit loading per square foot is higher (26.6 pounds) because of its smaller area. At a given air speed there is a large variation in the maximum loads

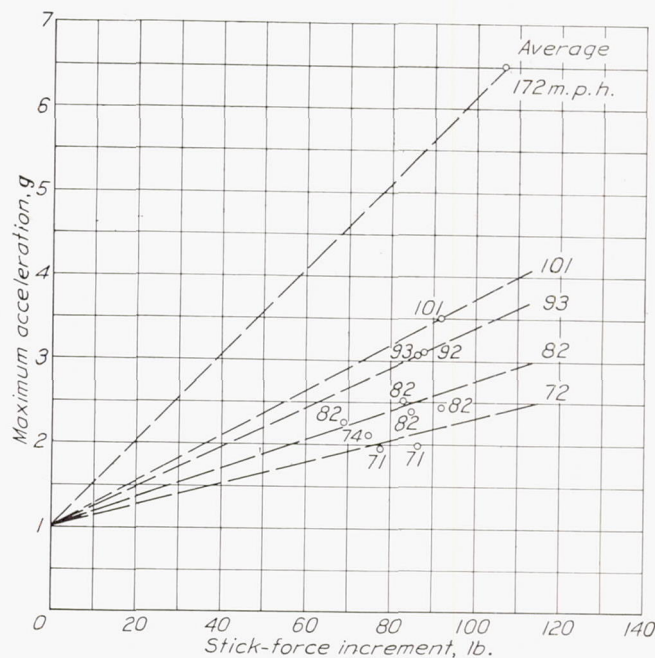


FIGURE 27.—Relation between acceleration and stick-force increment in abrupt pull-ups from level flight (modified tail). Numbers refer to air speed at start of pull-up.

measured that is due to slightly different rates of stick movement and to differences in the applied forces. Differences in the rate of stick movement are difficult

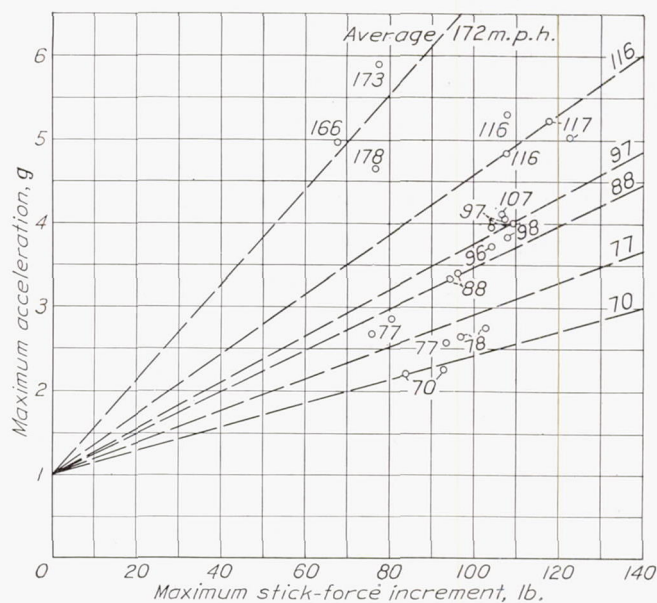


FIGURE 28.—Relation between acceleration and stick-force increment in abrupt pull-ups from level flight (original tail). Numbers refer to air speed at start of pull-up.

to detect because of the steep gradient of the control records.



An average line through the points of figure 25 would indicate that the maximum load obtained in the abrupt pull-ups varies nearly linearly with the air speed instead of as the square and, as a consequence, the normal-force coefficients increase inversely with the air speed.

The variation of the maximum acceleration in the abrupt pull-ups with the increment in stick force is plotted in figures 27 and 28 for the two tail surfaces with each point labeled for the air speed that existed at the start. The increment given is the difference between the maximum force recorded during the pull-up and the initial force on the stick prior to the maneuver. If straight lines are drawn, as indicated, through the average of each group of points for a given air speed and the 0-1*g* point, it is apparent that the increment of force required to produce a given acceleration increases with a decrease in air speed. Since no graduated pull-ups were made, the relation between acceleration and stick-force increment may not be linear as indicated by the lines in figures 27 and 28.

## II. PRESSURE DISTRIBUTION OVER THE RIGHT WING CELLULE AND SLIPSTREAM SECTIONS

### METHOD

The tests of the wing cellule were carried out in two parts in order to make the best use of the available pressure cells. In the first section, called the "wing hook-up," pressure measurements were taken on all ribs on the upper wing outboard of, and including, rib  $S_1$  and all ribs, excepting  $R_1$ , on the right lower wing (fig. 4). In the next section, called the "slipstream hook-up," pressure measurements were taken on ribs  $S_1$ , B, and H, in addition to all the ribs previously omitted. Thus ribs  $S_1$ , B, and H furnished a means for tying in the data between the two sections, a procedure simplified by making similar runs with the two arrangements.

The flight tests with each arrangement were divided into three groups consisting of: (1) a series of level-flight runs starting from just above stalling speed and increasing by approximately 10-mile-per-hour increments up to high speed, (2) a series of abrupt pull-ups and push-downs from level flight at the foregoing speeds, and (3) a series of abrupt right and left aileron rolls with rudder neutral at various speeds throughout the speed range. Several shallow dives at about 170 miles per hour were also made with the engine fully throttled.

The method of working up the results was somewhat similar to that employed in the tail-surface tests. For the symmetrical-loading conditions the rib-pressure curves were mechanically integrated to obtain the rib load and the rib moment about the wing leading edge. The rib loads and moments were then converted into coefficient form by the relations

$$(1) c_n = n/qc$$

$$(2) c_m = m_{l.e.}/qc^2$$

where

- $c_n$  is the rib normal-force coefficient.
- $n$ , rib load normal to chord, pounds per foot of span.
- $q$ , dynamic pressure, pounds per square foot.
- $m_{l.e.}$ , pitching moment about leading edge, foot-pounds per foot.
- $c_m$ , pitching-moment coefficient about leading edge.
- $c$ , rib chord, feet.

The rib loads were then plotted against their span location and the resulting curves integrated for total wing load. These loads were converted to individual wing and wing cellule normal-force coefficients from the relations

$$C_{N_U} = \frac{N_U}{qS_U}; \quad C_{N_L} = \frac{N_L}{qS_L}$$

and

$$\text{Cellule } C_N = \frac{C_{N_U}S_U + C_{N_L}S_L}{S_U + S_L}$$

where

$N_U$  and  $N_L$  are the integrated loads for upper and lower wings, pounds.

$S_U$  and  $S_L$  are the upper and lower wing areas, square feet. The lower wing area does not include the part intercepted by the fuselage.

In the aileron rolls, the rib-pressure curves were integrated for both load and moment but the results were not converted into coefficient form.

Since the tie-in rib  $S_1$  on the upper wing was some distance out from the center, it was necessary, in order to obtain the cellule and upper wing normal-force coefficients, to extend the span loadings to the wing center. In the symmetrical-flight conditions they were extending by plotting the values of the normal-force coefficients of the slipstream ribs against that of the tie-in rib. The span load for the upper wing was then continued by means of these intermediate plots together with the appropriate value of the normal-force coefficient for rib  $S_1$ . In the aileron rolls, the span loads were continued across the slipstream sections by interpolation between the partial-span load curves for the slipstream section by the use of the values of normal-force coefficients given by the tie-in ribs  $S_1$  and H.

### PRECISION

The individual rib pressures in the wing investigation are subject to the same errors listed for the tail pressures. The magnitudes of the different sources of error are the same with the exception of that due to width and haziness of the record lines, which is less for the wing tests. The errors in rib loads due to fairing are also smaller because of the larger number of orifices per rib.



The loads on the individual wings are believed to be correct to within 75 pounds and individual rib loads to within 7 pounds. A good idea of the accuracy of the load results may be obtained by noting the dispersion of the points in figures 33 and 34.

The air speeds in level flight are correct to within  $1\frac{1}{2}$  miles per hour. In the push-downs, pull-ups, and rolls, the air-speed head, although measuring the dynamic pressure at the head correctly to within 2 percent, does not record the correct dynamic pressures for calculating coefficients since the speed varies along the span. Control positions and control forces are believed accurate to within  $2^\circ$  and 3 pounds, respectively.

#### RESULTS AND DISCUSSION

**Symmetrical-flight condition.**—Results for the symmetrical-flight condition, which includes push-downs, pull-ups, dive pull-outs, and steady flight, are given in figures 29 to 35.

Typical span load and span  $c_n$  variations are given in figure 29 for steady flight at air speeds ranging from 58 to 171 miles per hour. The span loadings over the upper wing in level flight (fig. 29 (a)) show comparatively little variation with air speed. At the center the loads tend to be low owing to the center-section cut-out; also, owing to a clockwise rotation of the slipstream, there is a tendency for the loads just to the right of the center line to be lower than those to the left. The load curves for the lower wing show a similar but increased slipstream effect, which is due to the low position of the thrust line. Although the rotation effect is present on the wings, the tests of the tail surfaces indicated that there it had been practically damped out since little dissymmetry of load occurred.

In the throttled dive (fig. 29 (a)) the span loading is much more irregular than in the level-flight condition owing to the fact that a negative thrust is present and that the wing had a slight twist, the effect of a small twist on the load being much more noticeable at the smaller wing lift coefficients. Measurements of the profiles of the extreme tip ribs (G and N) on both wings showed them to be at a smaller effective angle than those farther inboard while ribs F and M were found to be at a higher angle. This twist at the tip was due to the fairing used in forming the rounded portion of the wing, although there may also have been an actual twist of the wing structure in flight.

The curves given by figure 29 (b) indicate that the  $c_n$  values at the center tend to be high, even though these sections are effectively washed out with respect to the rest of the wing, because of the tendency for the lift to be maintained across a cut-out. This washout arises from the fact that the ribs in the center section were formed by simply cutting off the trailing edge of a Göttingen 398 airfoil and fairing in the bottom surface, as shown by figure 4.

The distribution of load on the individual wing ribs

is given in figure 30 where the local pressures are given in terms of the dynamic pressure at the air-speed head. These distributions, which correspond to some of the previous span-loading curves, are similar to those obtained in other investigations and require no comment as to their shape. It will be noted, however, that the pressures at the leading edge show a peculiar variation, indicating that there the flow is extremely critical.

Although figures 29 and 30 showed typical results for the load distribution, the final averaged results for the symmetrical-flight condition are contained in figures 31 and 32. The results of these figures, which give the variation of rib  $c_n$  with individual wing  $C_N$  and of rib  $c_m$  with rib  $c_n$  respectively, were determined from curves similar to those given in figures 33 and 34, which indicate both the average scattering and the number of experimental points used to establish each of the curves given in figures 31 and 32. It will be noted (figs. 31 and 32) that ribs  $S_2$  and  $S_3$  show two distinct curves at the higher lift coefficients. The points that form the second, or dotted, curve occurred in some but not all of the pull-ups. An analysis of the points determining the two curves showed no tendency for one curve to be associated with pull-ups at one end of the speed range or vice versa; also, since these pull-ups were made from power-on flight, a difference in slipstream conditions was not an explanation. The only cause to which this peculiar flow could be attributed was that the flow past the top of the fuselage nose, which incidentally had louvers, was critical to the shutter opening on the radiator.

In these tests the maximum individual wing  $C_N$  measured was 1.9 (upper wing); the maximum individual rib  $c_n$  values measured were over 2.1 for ribs  $S_2$ ,  $S_3$ , and  $S_A$ . These high values are common in abrupt maneuvers and occur if the angular velocity in pitch is sufficiently great to carry the lift past the normal burble angle before the wing stalls.

The relative efficiency of the wings is given in figure 35 where the ratio  $C_{N_U}/C_{N_L}$  is plotted against the cellule  $C_N$ . These curves were determined from the results of an integration of individual wing-load curves, known wing areas, and an air speed measured one chord length ahead of the upper wing. It is obvious, however, that in a pull-up or push-down the wings are actually traveling at different air speeds owing to the angular velocity in pitch and that the effect, if a single air speed is used, is to change the apparent relative efficiencies between the wings of a biplane. Figure 35 shows three distinct curves, rather than a series of transition curves, because the points determining them were obtained from records that were read near or at the peak loads, which occur practically simultaneously with the maximum angular velocity. If the records had been read at intervening time intervals, a gradual transition from the level-flight to the pull-up curve would have been indicated.



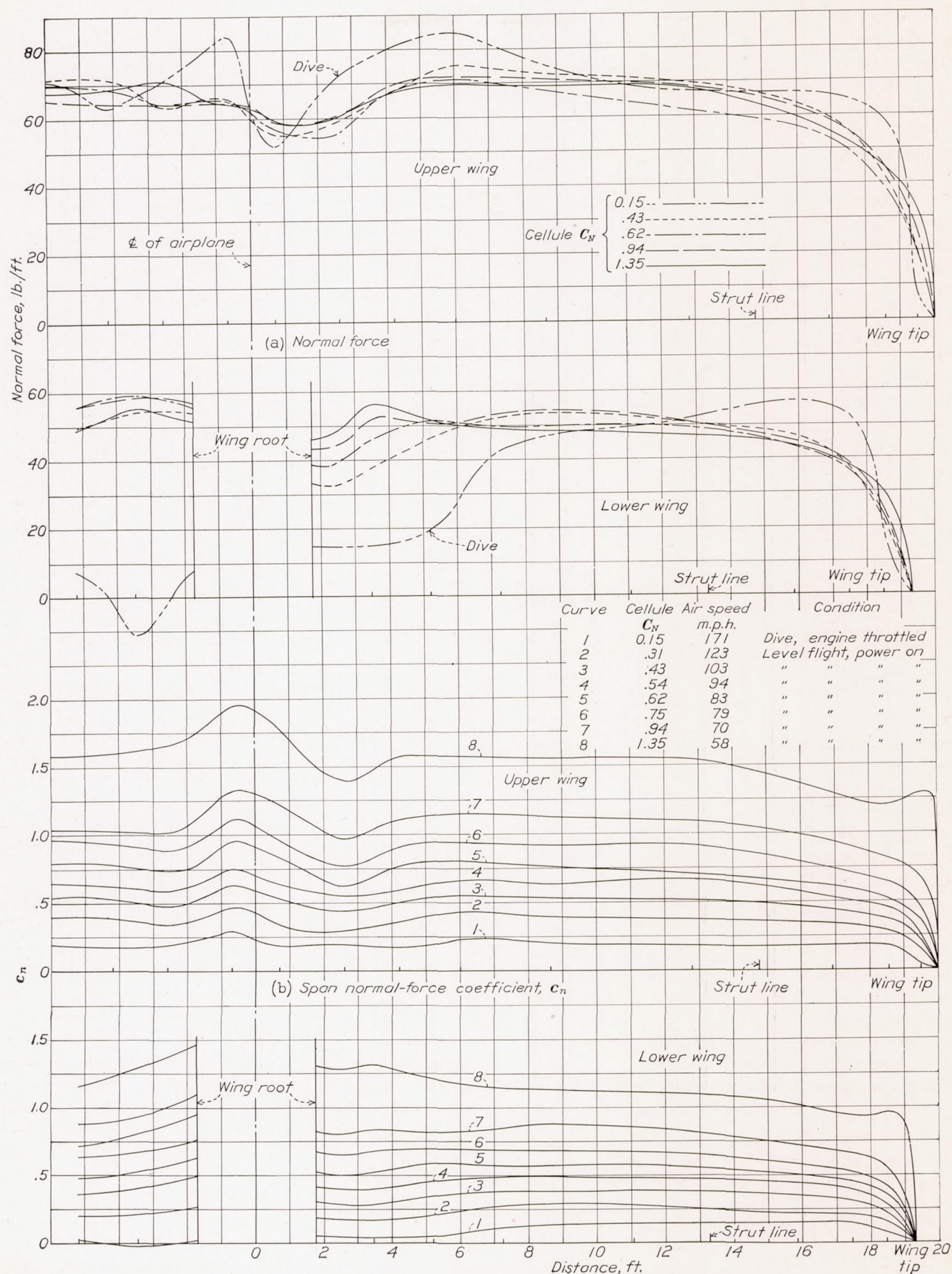


FIGURE 29.—Distribution of normal force and normal-force coefficient along the wing span.



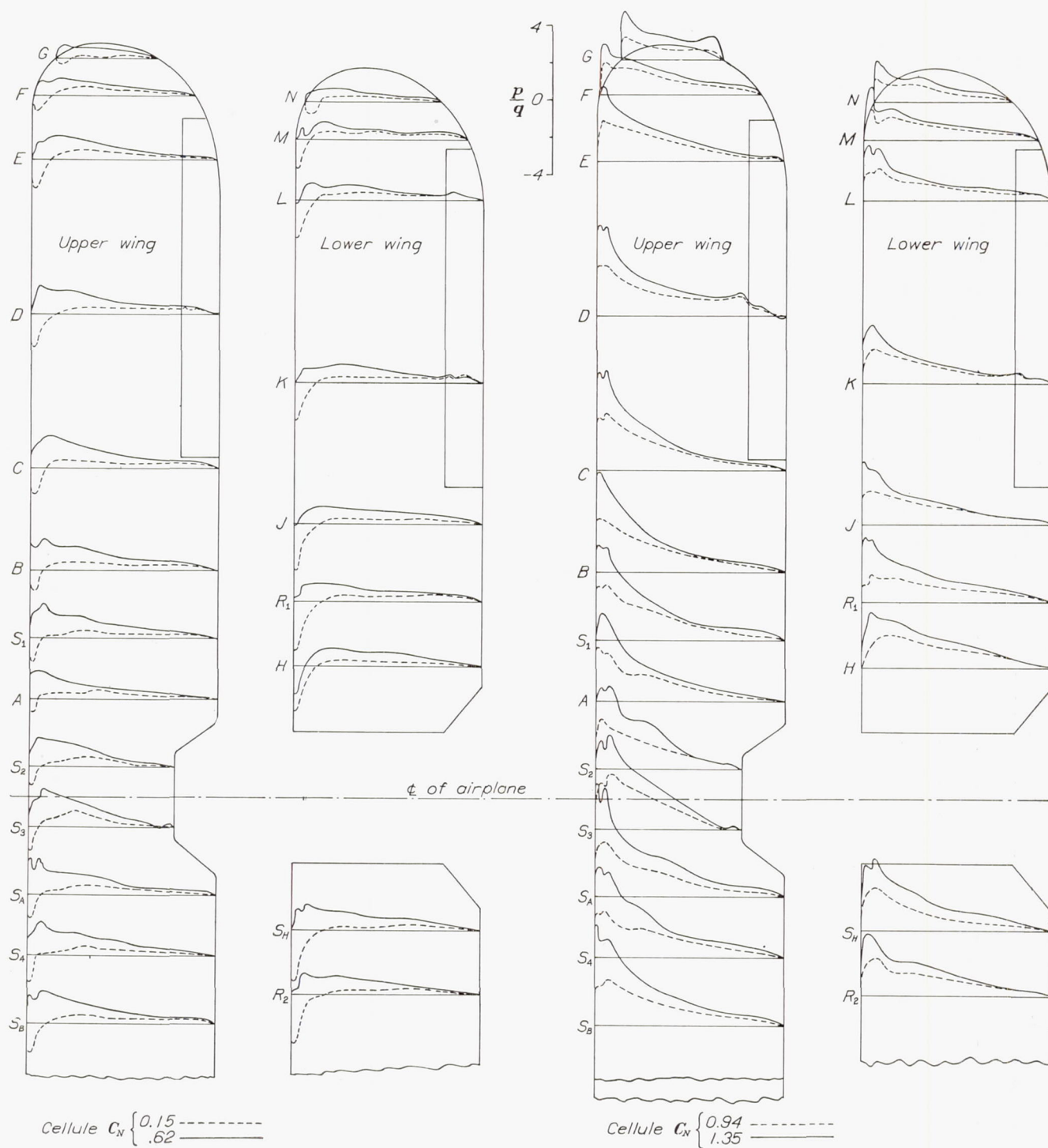
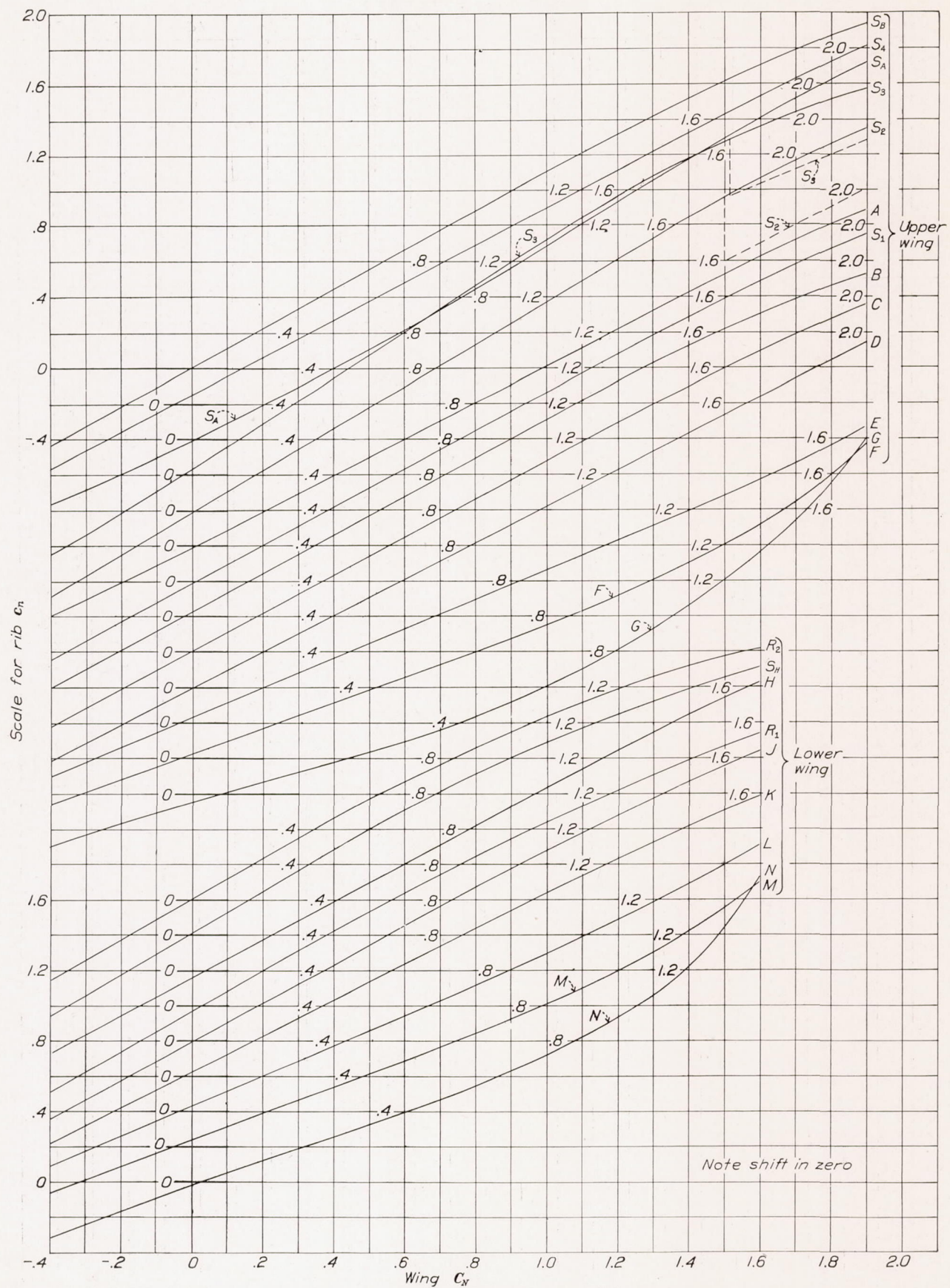
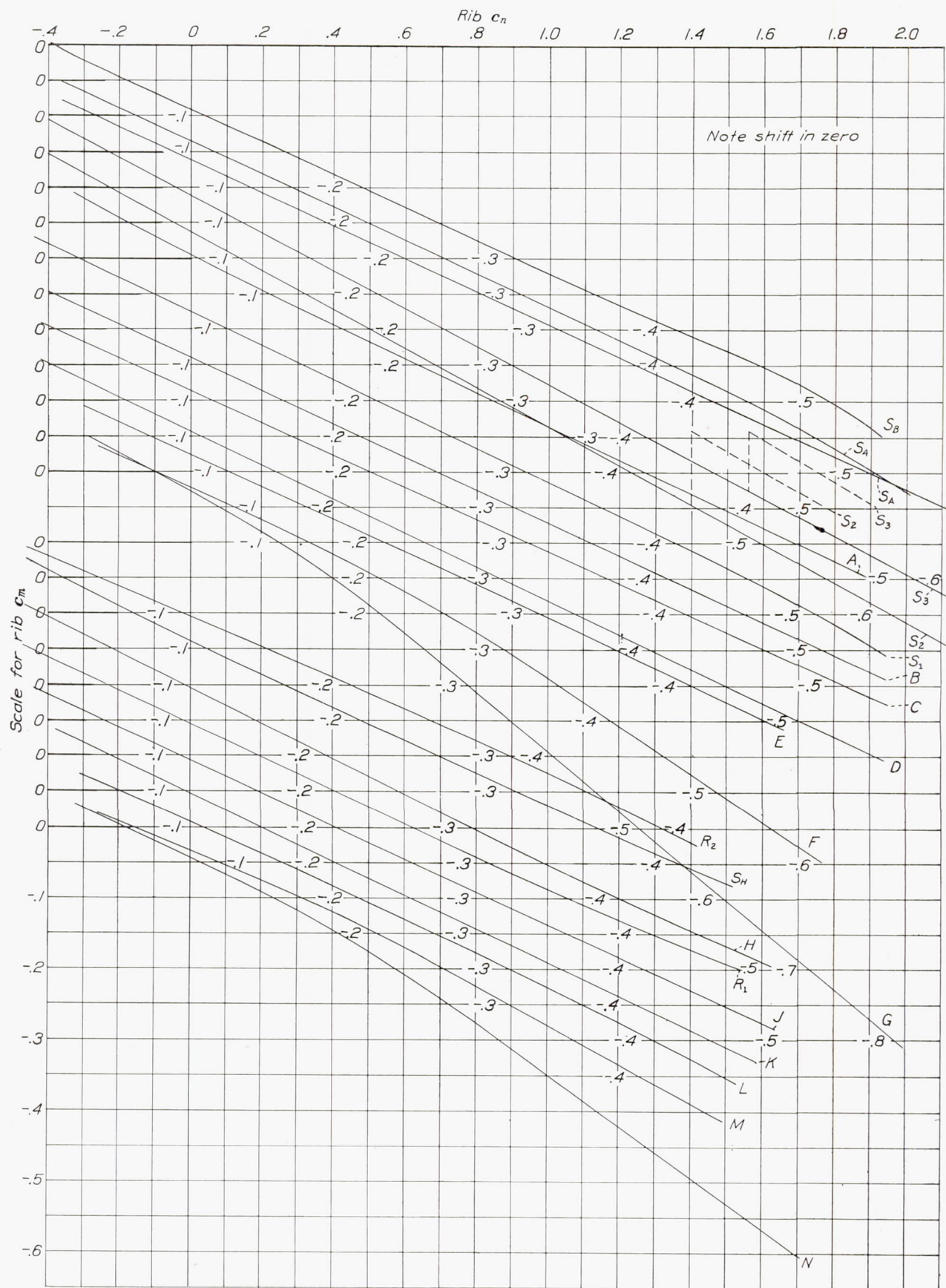


FIGURE 30.—Rib pressure distribution in steady flight.







FIGURE 32.—Variation of rib  $c_m$  with rib  $c_n$ .



In order to reconstruct the span  $c_n$  or  $c_m$  distributions obtained in the symmetrical-flight conditions a cellule coefficient is first chosen and reference made to figure 35 to find the relative efficiency. With this ratio and the formula

$$\text{Cellule } C_N = \frac{C_{N_U} S_U + C_{N_L} S_L}{S_U + S_L}$$

the individual wing  $C_N$  values may be found. Figures 31 and 32 are then referred to for the variation of rib  $c_n$  and  $c_m$  along the span.

**Aileron rolls.**—The results of the aileron rolls are given in figures 36 to 41 and in table II. Time histories of the measured quantities are given in figures 36 and 37 for 6 right and 6 left aileron rolls made at various air speeds. Figures 38 to 40 give the variation with time of the span load distribution, rib load distribution, and individual wing load during abrupt right and left aileron rolls at 120 miles per hour. These results, which correspond to runs 43 and 39 (figs. 36 and 37), are typical of those measured at other speeds. The maximum measured air loads on aileron ribs D and K are given in figure 41. The wing rib characteristics,

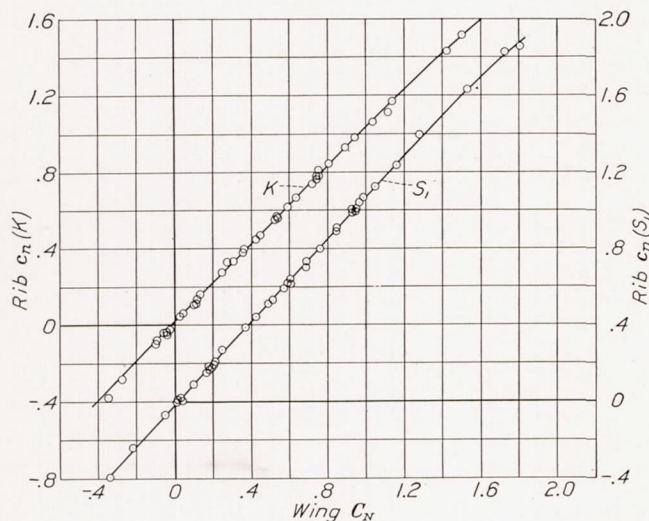


FIGURE 33.—Typical wing rib  $c_n$  curves showing scattering of experimental points for ribs  $S_1$  and  $K$ .

i. e., rib loads, rib moments about the leading edge, and rib centers of pressure, are tabulated in table II for all the aileron rolls.

The irregularity of the span-load curves in the roll (fig. 38) is due to the combination of an effective twist introduced by deflecting the ailerons and a twist introduced by the subsequent rolling motion. In a left roll, the load on the right wing is first increased owing to the down aileron; then, as the airplane rolls, the load decreases owing to the rolling action and also to the decrease of the component of airplane weight normal

to the span. In a right roll, the load on the right wing is first decreased by the aileron action; subsequently it tends to increase as rolling occurs and finally to decrease as the lift component becomes smaller. This variation is indicated both by the time histories of the accelerometer mounted inside the wing near the tip (figs. 36 and 37) and by the results shown in figure 40.

The load distribution over the aileron ribs (fig. 39) indicates that the peak pressure at the leading edge of the aileron is greater during the left aileron roll than during the right. This variation is due to a smaller aileron deflection and is shown in figures 36 and 37. Since the ailerons had no differential action, the smaller deflection is a direct result of piloting technique.

The results shown in figure 41 indicate that the loads measured on aileron ribs D and K tend to increase

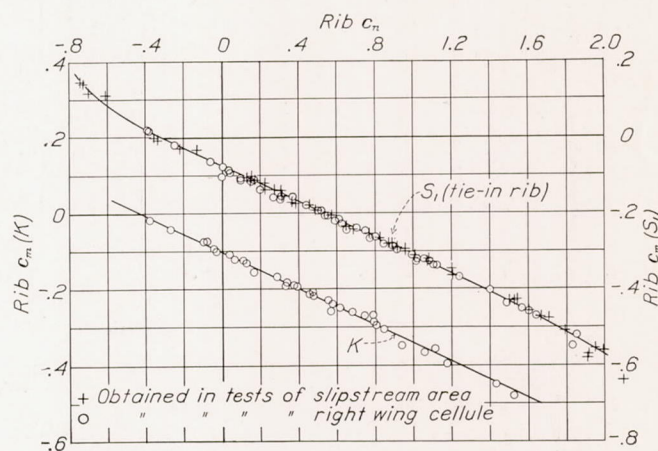


FIGURE 34.—Typical wing rib  $c_m$  curves showing scattering of experimental points for ribs  $S_1$  and  $K$ .

linearly with initial air speed as did the maximum load on the tail surfaces in the abrupt pull-ups. The load on the upper aileron rib (rib D) is larger than that on the lower aileron rib regardless of the direction of deflection. Since the resultant load on the aileron is upward for zero deflection (fig. 30), the magnitude of the up loads with the aileron down is greater than the corresponding down loads when the aileron is up.

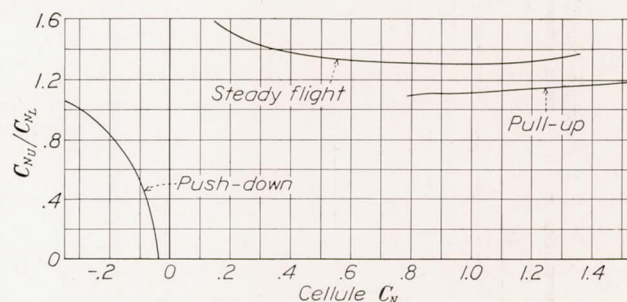


FIGURE 35.—Relative efficiency of upper and lower wings.



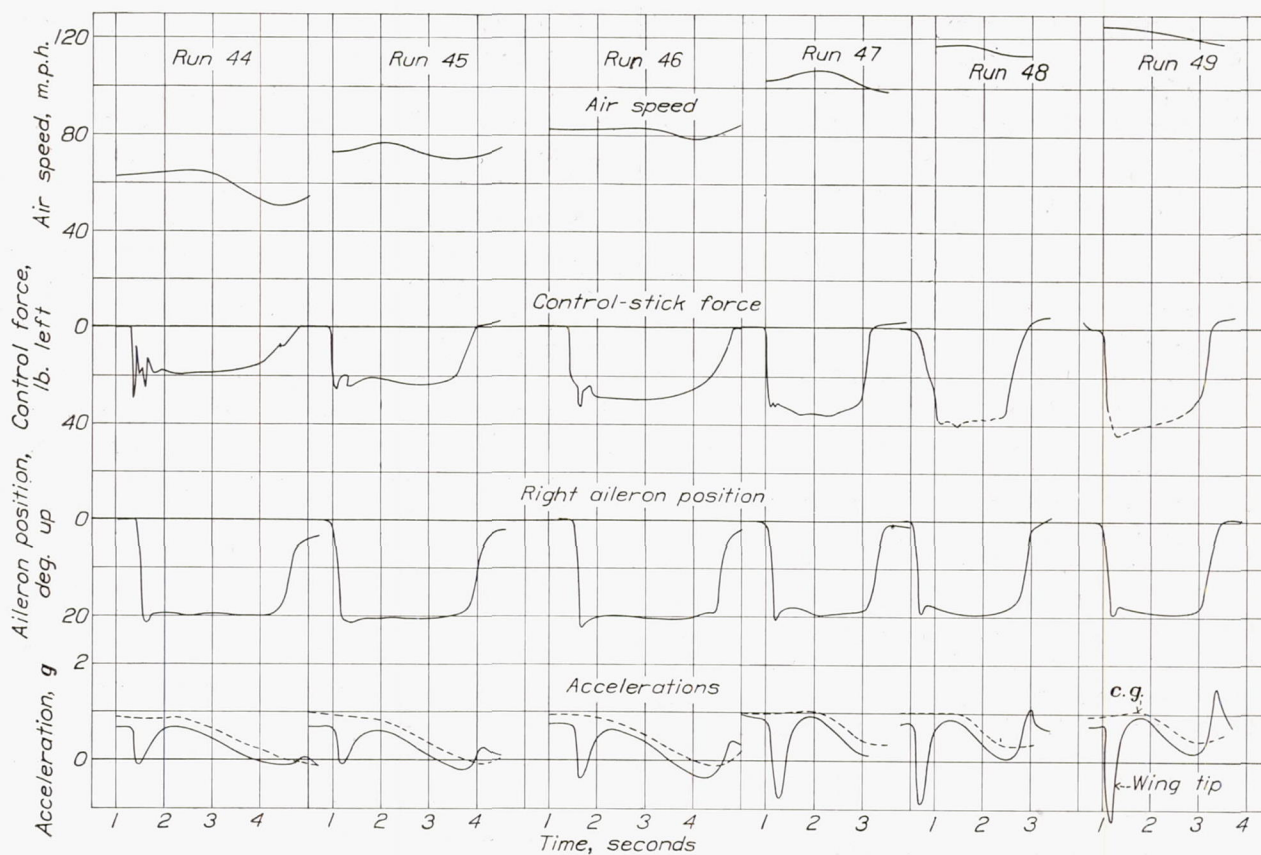


FIGURE 36.—Time histories of six right aileron rolls.

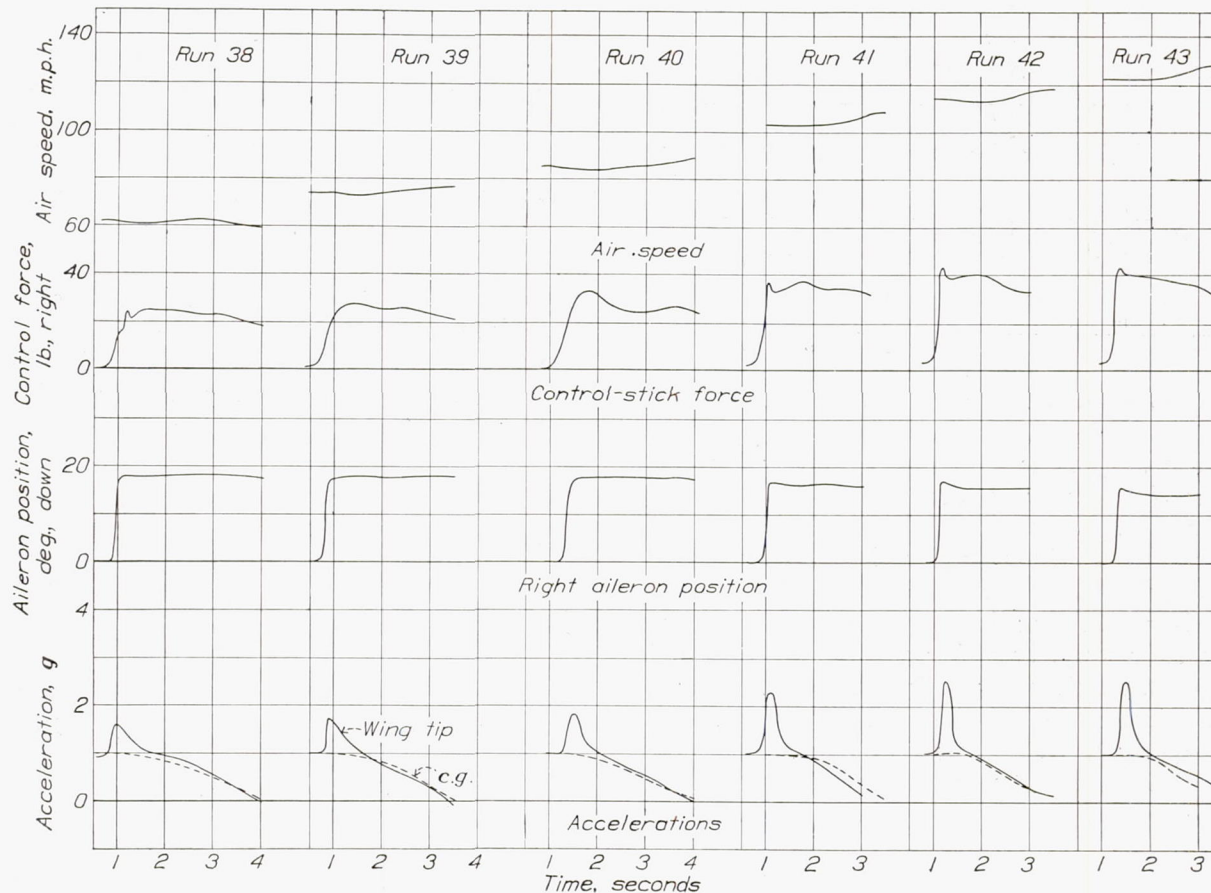


FIGURE 37.—Time histories of six left aileron rolls.



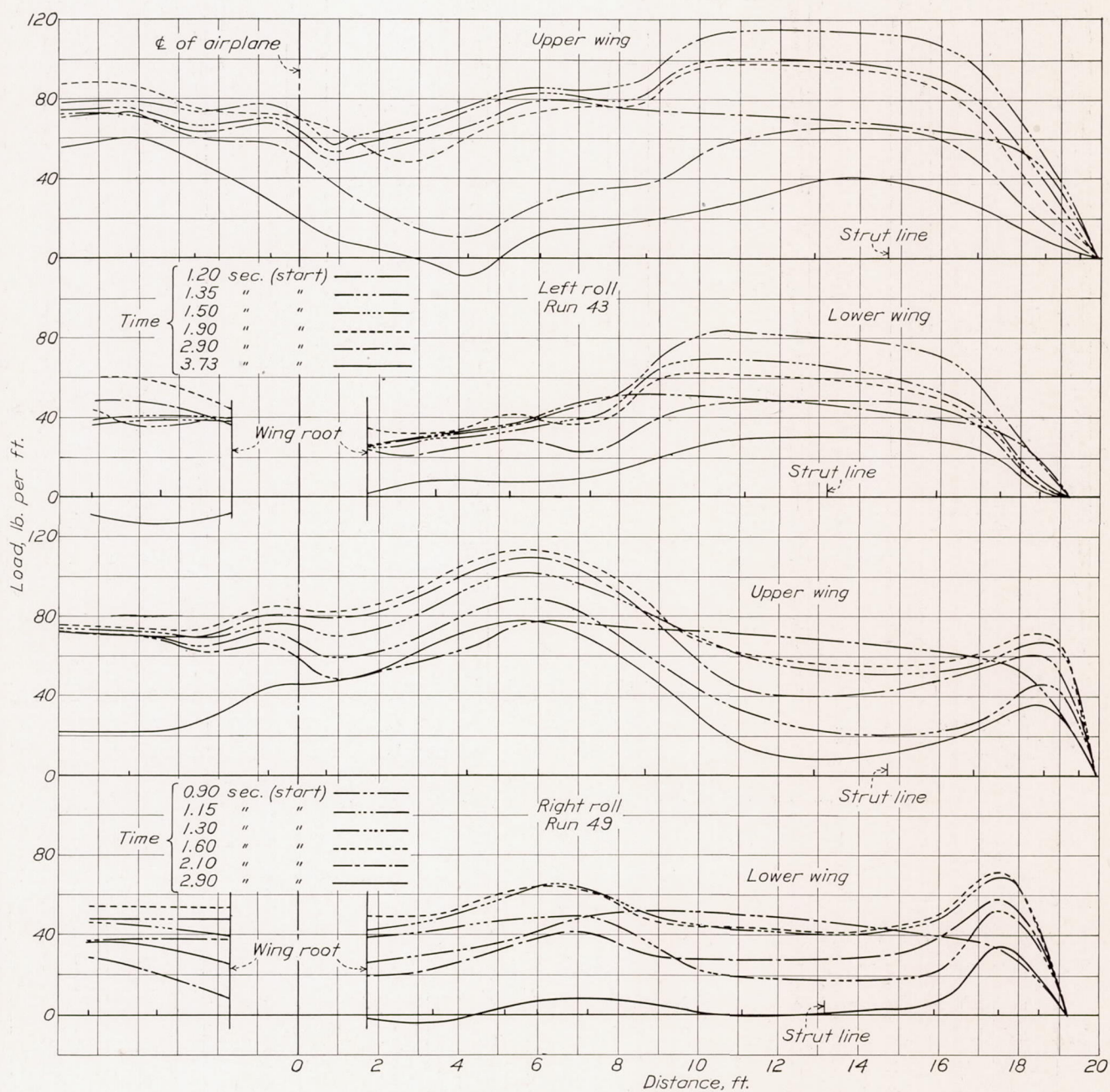


FIGURE 38.—Distribution of normal force along wing span obtained in abrupt aileron rolls at 120 miles per hour.



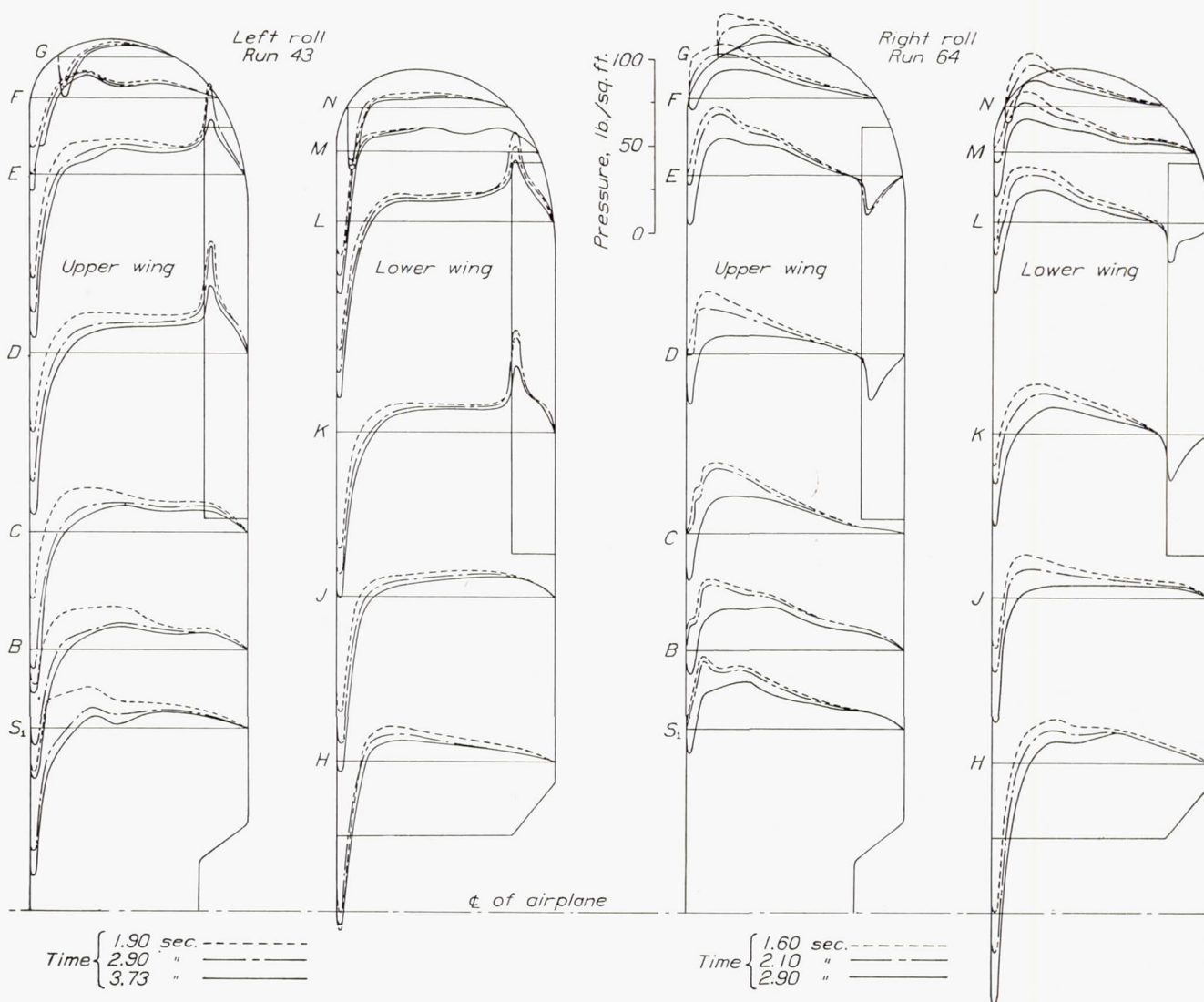


FIGURE 39.—Rib pressure distribution over the upper and lower wings during abrupt aileron rolls at 120 miles per hour.

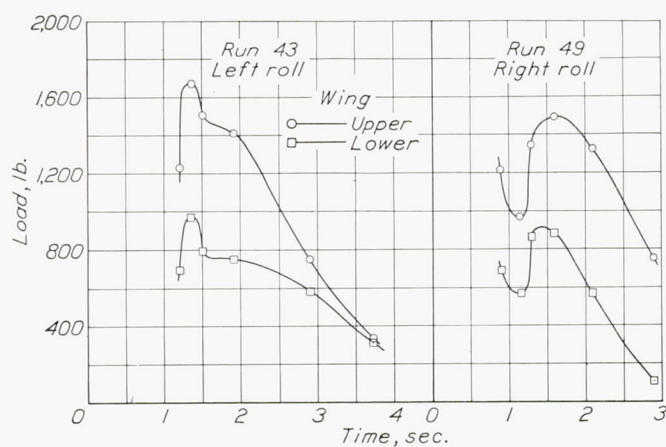


FIGURE 40.—Variation of individual wing loads measured in abrupt aileron rolls at 120 miles per hour.

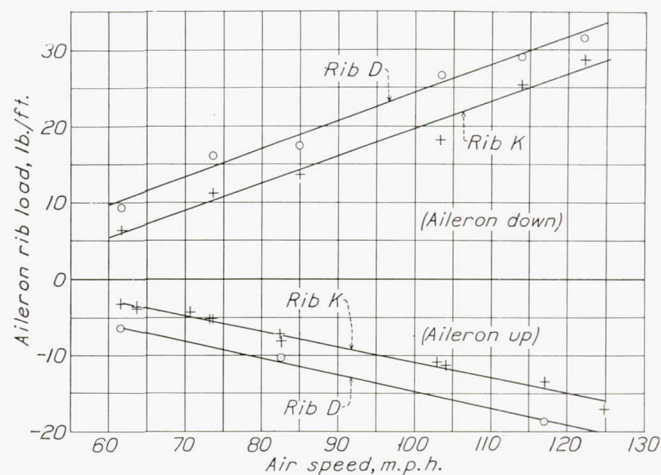


FIGURE 41.—Aileron rib load in abrupt aileron rolls.



## CONCLUSIONS

The pressure-distribution tests over the two tail surfaces showed that:

1. Although for large elevator deflections horn-type balances performed their intended function of reducing hinge moments, they actually increased the hinge moment for small deflections.

2. The difference in the load on the two sides of the tail surfaces due to slipstream rotation was of minor importance.

3. The tail moment in the steady dive was calculated with fair accuracy by static-equilibrium equations that took into account the moments exerted by the wing and fuselage.

4. In abrupt pull-ups the maximum up tail loads may be as great as the maximum down tail loads.

5. In abrupt pull-ups the maximum tail normal-force coefficients developed decreased with an increase in air speed.

6. The acceleration produced with a given increment of stick force increased with the initial air speed.

The pressure-distribution tests over the right wing cellule and slipstream area showed that:

1. The effective relative efficiency between biplane wings varied considerably with the type of maneuver.

2. The maximum unsymmetrical load in the abrupt aileron roll occurred as soon as the aileron reached its maximum deflection.

3. The unit loadings on the ailerons of a biplane are affected by the relative efficiency between the wings.

LANGLEY MEMORIAL AERONAUTICAL LABORATORY,  
NATIONAL ADVISORY COMMITTEE FOR AERONAUTICS,  
LANGLEY FIELD, VA., December 8, 1936.

## REFERENCES

1. Rhode, Richard V.: The Pressure Distribution over the Wings and Tail Surfaces of a PW-9 Pursuit Airplane in Flight. T. R. No. 364, N. A. C. A., 1930.
2. Theodorsen, Theodore: Investigation of the Diaphragm-Type Pressure Cell. T. R. No. 388, N. A. C. A., 1931.
3. Roche, J. A.: Study of Balanced Rudders. A. C. I. C. No. 586, Matériel Division, Army Air Corps, 1927.
4. Rhode, Richard V., and Lundquist, Eugene E.: Pressure Distribution over the Fuselage of a PW-9 Pursuit Airplane in Flight. T. R. No. 380, N. A. C. A., 1931.

TABLE I

## CHARACTERISTICS OF DOUGLAS O-2H AIRPLANE

Engine—Liberty.....	420 hp. at 1,750 r. p. m.
Airfoil.....	Göttingen 398
Weight during pressure-distribution measurements of—	
Modified tail.....	4,660 lb.
Original tail.....	4,736 lb.
Wing cellule.....	4,708 lb.
Areas:	
Upper wing.....	190.4 sq. ft.
Lower wing.....	182.4 sq. ft.
Total.....	372.8 sq. ft.
Elevator, modified tail (including 2.06-square-foot balance).....	27.00 sq. ft.
Stabilizer, modified tail.....	23.82 sq. ft.
Total horizontal surfaces, modified tail.....	50.82 sq. ft.
Elevator, original tail (including 4.53-square-foot balance).....	25.70 sq. ft.
Stabilizer, original tail.....	21.24 sq. ft.
Total horizontal surfaces, original tail.....	46.94 sq. ft.
Rudder, all tests (including 0.93-square-foot balance).....	11.81 sq. ft.
Fin, all tests.....	6.41 sq. ft.
Total vertical tail surfaces.....	18.22 sq. ft.
c. g. location back of leading edge of lower wing during tests:	
Modified tail.....	8.20 in.
Original tail.....	9.55 in.
Wing cellule.....	6.80 in.
G/c.....	1.2
Stagger.....	17° or 22 in.
Dihedral.....	2°
Decalage.....	0.
Incidence.....	2°
Thrust-line location above leading edge of lower wing.....	2 ft. 1.4 in.
Distance from leading edge of lower wing to center line of tail-hinge axis.....	20 ft. 3 in.
Tail-hinge location above thrust line.....	2 ft. 0 in.



TABLE  
WING RIB LOADS AND MOMENTS

Time, sec.	Rib	Run 38 (air speed 62 m. p. h. <sup>1</sup> )									Run 39 (air speed 74 m. p. h. <sup>1</sup> )									Run 40 (air speed 85 m. p. h. <sup>1</sup> )								
		Rib load, lb.			Rib moment, lb.-ft.			c. p. from leading edge, ft.			Rib load, lb.			Rib moment, lb.-ft.			c. p. from leading edge, ft.			Rib load, lb.			Rib moment, lb.-ft.			c. p. from leading edge, ft.		
		1.09	1.90	2.50	1.09	1.90	2.50	1.09	1.90	2.50	0.90	1.90	2.50	0.90	1.90	2.50	0.90	1.90	2.50	1.40	2.09	2.90	1.40	2.09	2.90	1.40	2.09	2.90
S <sub>B</sub>	77	77	72	-112	-99	-95	1.45	1.28	1.32	84	69	60	-125	-107	-98	1.49	1.55	1.63	98	83	63	-156	-137	-111	1.59	1.65	1.76	
S <sub>4</sub>	75	75	70	-109	-97	-93	1.45	1.29	1.33	84	69	62	-126	-108	-99	1.50	1.56	1.60	94	79	62	-144	-125	-105	1.53	1.58	1.66	
S <sub>3</sub>	81	80	72	-117	-103	-93	1.45	1.29	1.29	82	67	56	-124	-104	-90	1.51	1.55	1.61	89	74	58	-137	-118	-99	1.54	1.60	1.71	
S <sub>2</sub>	73	73	65	-92	-76	-62	1.26	1.04	.95	75	55	40	-94	-70	-49	1.25	1.27	1.22	82	67	46	-105	-86	-61	1.28	1.28	1.33	
A <sub>1</sub>	67	67	56	-91	-74	-55	1.36	1.10	.98	64	32	22	-85	-60	-36	1.33	1.87	1.64	68	53	26	-99	-80	-47	1.45	1.51	1.81	
A <sub>2</sub>	63	63	54	-88	-74	-63	1.40	1.17	1.17	65	29	16	-93	-66	-38	1.43	2.27	2.37	68	53	26	-116	-92	-91	1.71	1.74	3.50	
B	72	60	38	-109	-92	-70	1.51	1.53	1.84	73	45	14	-112	-81	-44	1.53	1.80	3.14	70	56	16	-120	-101	-56	1.71	1.74	3.50	
C	75	64	44	-117	-103	-77	1.56	1.61	1.75	76	52	21	-120	-96	-58	1.58	1.85	2.76	77	63	24	-137	-116	-71	1.78	1.84	2.96	
D	76	63	47	-119	-101	-87	1.57	1.60	1.85	78	54	28	-129	-106	-78	1.65	1.96	2.78	78	65	31	-142	-129	-95	1.82	1.98	3.06	
E	80	71	58	-153	-147	-120	1.91	2.07	2.07	92	68	46	-193	-156	-129	2.10	2.30	2.81	94	78	54	-213	-191	-168	2.26	2.45	3.11	
F	64	54	42	-126	-112	-89	1.97	2.08	2.12	74	51	32	-158	-125	-103	2.14	2.45	3.22	74	57	38	-175	-153	-132	2.36	2.68	3.47	
G	40	32	25	-64	-49	-38	1.60	1.53	1.52	42	26	17	-65	-44	-36	1.55	1.69	2.12	40	29	19	-68	-56	-45	1.70	1.93	2.37	
H	22	16	10	-24	-17	-9	1.09	1.06	.90	23	9	6	-22	-9	-4	.96	1.00	.67	19	10	7	-20	-11	-8	1.05	1.10	1.14	
R <sub>2</sub>	58	42	35	-94	-65	-54	1.62	1.55	1.54	57	38	17	-94	-72	-33	1.65	1.90	1.94	59	51	23	-119	-95	-54	2.02	1.86	2.35	
R <sub>1</sub>	65	44	37	-102	-69	-55	1.57	1.57	1.49	64	41	15	-102	-77	-28	1.59	1.88	1.87	63	55	20	-125	-99	-53	1.98	1.80	2.65	
H	54	55	49	-100	-101	-89	1.85	1.84	1.81	52	44	33	-102	-90	-67	1.96	2.04	2.03	52	43	32	-122	-102	-77	2.35	2.37	2.41	
J	55	60	53	-98	-112	-101	1.78	1.87	1.91	54	47	36	-101	-97	-62	2.02	2.06	2.39	55	46	31	-120	-103	-91	2.18	2.24	2.94	
K	53	51	50	-95	-90	-94	1.79	1.76	1.88	54	46	39	-98	-94	-96	1.81	2.04	2.46	53	49	42	-111	-109	-112	2.09	2.22	2.66	
L	51	46	42	-104	-96	-89	2.04	2.09	2.12	63	50	34	-141	-123	-101	2.24	2.46	2.97	65	37	41	-164	-109	-134	2.52	2.95	3.27	
M	46	43	40	-97	-92	-86	2.11	2.14	2.15	57	41	34	-129	-106	-100	2.26	2.59	2.94	58	44	37	-142	-128	-127	2.45	2.91	3.43	
N	34	31	29	-61	-56	-52	1.79	1.81	1.79	40	28	22	-70	-60	-53	1.75	2.14	2.41	38	29	25	-78	-71	-69	2.05	2.45	2.76	
	18	15	12	-28	-20	-17	1.55	1.33	1.42	22	12	8	-30	-19	-15	1.36	1.58	1.87	19	12	10	-28	-22	-18	1.47	1.83	1.80	

Time, sec.	Rib	Run 44 (air speed 63 m. p. h. <sup>1</sup> )									Run 45 (air speed 74 m. p. h. <sup>1</sup> )									Run 46 (air speed 83 m. p. h. <sup>1</sup> )								
		Rib load, lb.			Rib moment, lb.-ft.			c. p. from leading edge, ft.			Rib load, lb.			Rib moment, lb.-ft.			c. p. from leading edge, ft.			Rib load, lb.			Rib moment, lb.-ft.			c. p. from leading edge, ft.		
		1.40	2.10	3.90	1.40	2.10	3.90	1.40	2.10	3.90	1.10	1.90	2.90	1.10	1.90	2.90	1.10	1.90	2.90	1.60	2.15	3.10	1.60	2.15	3.10	1.60	2.15	3.10
S <sub>B</sub>	61	66	11	-106	-105	-46	1.74	1.59	4.18	58	63	33	-101	-109	-76	1.74	1.73	2.30	55	63	34	-108	-120	-87	1.96	1.91	2.56	
S <sub>4</sub>	60	65	12	-104	-103	-47	1.73	1.58	3.92	52	57	28	-86	-94	-61	1.65	1.65	2.18	56	62	34	-105	-116	-82	1.87	1.87	2.41	
S <sub>3</sub>	67	72	24	-106	-105	-56	1.58	1.46	2.33	61	66	38	-99	-107	-73	1.62	1.62	1.92	58	65	38	-100	-112	-79	1.72	1.72	2.08	
S <sub>2</sub>	67	71	28	-89	-88	-43	1.33	1.24	1.53	63	68	43	-83	-91	-61	1.32	1.34	1.42	59	66	43	-81	-92	-63	1.37	1.39	1.46	
A <sub>1</sub>	58	63	28	-85	-84	-36	1.46	1.33	1.29	57	62	41	-83	-91	-61	1.46	1.47	1.49	64	71	50	-96	-107	-76	1.50	1.51	1.52	
A <sub>2</sub>	66	70	43	-94	-93	-63	1.42	1.33	1.46	62	67	50	-86	-94	-70	1.39	1.40	1.40	63	70	56	-98	-109	-87	1.55	1.56	1.55	
B	72	77	43	-106	-105	-72	1.47	1.36	1.67	75	80	59	-114	-121	-95	1.52	1.51	1.61	75	83	64	-122	-133	-109	1.63	1.60	1.70	
C	64	69	30	-83	-89	-45	1.30	1.29	1.50	80	84	59	-126	-130	-101	1.57	1.55	1.71	81	88	66	-135	-143	-115	1.67	1.62	1.74	
D	50	59	13	-43	-53	-6	.86	.90	.46	66	69	41	-89	-90	-64	1.35	1.30	1.56	64	73	48	-89	-101	-74	1.39	1.38	1.54	
E	40	49	15	-31	-44	-8	.77	.90	.53	51	57	21	-40	-48	-11	.78	.84	.52	43	55	21	-28	-42	-8	.65	.76	.38	
F	40	50	19	-54	-65	-32	1.35	1.30	1.68	40	49	27	-58	-68	-42	1.45	1.39	1.55	39	54	32	-58	-73	-48	1.49	1.35	1.50	
G	28	40	17	-30	-47	-20	1.07	1.17	1.18	25	36	20	-28	-41	-24	1.12	1.14	1.20	24	35	22	-25	-40	-26	1.04	1.14	1.18	
R <sub>2</sub>	60	53	28	-98	-81	-52	1.63	1.53	1.86	65	53	34	-116	-99	-55	1.78	1.86	1.62	63	59	33	-128	-125	-60	2.03	2.12	1.82	
H	67	60	20	-104	-87	-36	1.55	1.45	1.80	64	51	28	-106	-88	-37	1.66	1.73	1.32	63	59	28	-118	-115	-40	1.87	1.95	1.43	
H	56	49	-11	-102	-86	-6	1.82	1.75	-.54	54	42	2	-113	-96	-35	2.09	2.28	17.50	51	47	1	-115	-111	-17	2.26	2.36	17.00	
J	55	48	-5	-94	-77	-10	1.71	1.60	-2.00	57	45	8	-105	-88	-28	1.84	1.95	3.50	63	58	12	-128	-125	-30	2.03	2.16	2.50	
K	46	47	4	-69	-67	-14	1.50	1.42	3.50	49	43	12	-84	-70	-30	1.71	1.63	2.50	47	48	16	-85	-84	-40	1.81	1.75	2.50	
L	34	39	4	-30	-37	3	.88	.95	-.75	34	35	9	-34	-30	-3	1.00	.86	.33	29	36	12	-20	-25	-1	.69	.69	.08	
M	31	40	5	-22	-32	7	.71	.80	-1.40	28	35	10	-21	-24	4	.75	.69	-.40	27	37	10	-11	-20	-10	.41	.54	1.00	
N	40	44	15	-61	-64	-29	1.52	1.45	1.93	38	44	21	-60	-67	-36	1.58	1.52	1.71	39	48	25	-64	-74	-44	1.64	1.54	1.76	
	31	39	12	-38	-47	-17	1.22	1.21	1.42	30	37	17	-34	-44	-22	1.13	1.19	1.29	29	39	20	-33	-47	-26	1.14	1.20	1.30	

<sup>1</sup> Denotes air speed at start.



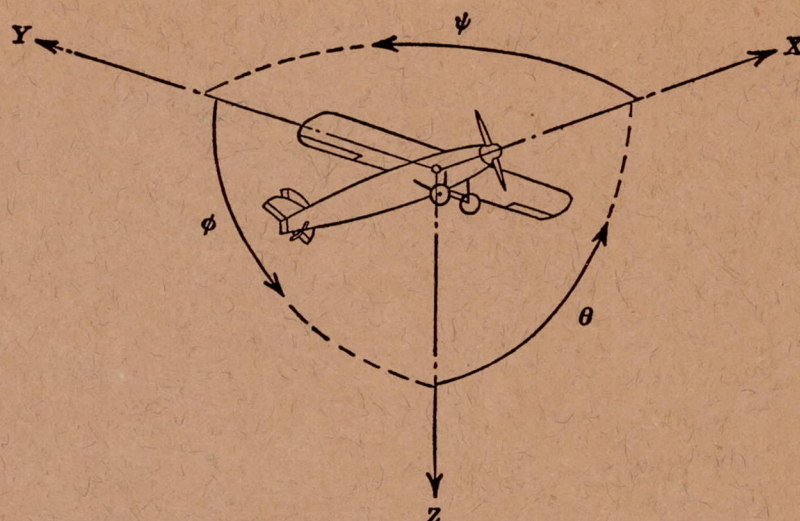
## II

## DURING AILERON ROLLS

Run 41 (air speed 103 m. p. h. <sup>1</sup> )									Run 42 (air speed 114 m. p. h. <sup>1</sup> )									Run 43 (air speed 122 m. p. h. <sup>1</sup> )									Time sec.	Rib
Rib load, lb.			Rib moment, lb.-ft.			c. p. from leading edge, ft.			Rib load, lb.			Rib moment, lb.-ft.			c. p. from leading edge, ft.			Rib load, lb.			Rib moment, lb.-ft.			c. p. from lead- ing edge, ft.				
1.93	2.92	3.38	1.93	2.92	3.38	1.93	2.92	3.38	1.90	2.92	3.53	1.90	2.92	3.53	1.90	2.92	3.53	1.90	2.90	3.73	1.90	2.90	3.73	1.90	2.90	3.73		
88	57	30	-161	-121	-116	1.83	2.12	3.87	84	60	46	-162	-149	-145	1.93	2.48	3.15	88	71	55	-182	-158	-151	2.07	2.23	2.75	S <sub>B</sub>	
86	64	35	-154	-135	-134	1.79	2.11	3.83	83	52	49	-151	-142	-140	1.82	2.73	2.86	87	73	60	-176	-155	-150	2.02	2.12	2.50	S <sub>4</sub>	
74	54	28	-131	-113	-112	1.77	2.09	4.00	72	49	46	-126	-113	-111	1.75	2.31	2.41	75	60	48	-148	-127	-122	1.97	2.12	2.54	S <sub>A</sub>	
69	38	12	-97	-59	-55	1.41	1.55	4.58	65	38	35	-88	-67	-64	1.35	1.76	1.83	72	58	29	-111	-81	-71	1.54	1.40	2.45	S <sub>3</sub>	
53	11	-15	-101	-52	-46	1.91	4.73	-3.07	55	17	13	-96	-58	-56	1.74	3.41	4.31	65	40	11	-112	-76	-62	1.72	1.90	5.64	S <sub>2</sub>	
57	16	-16	-134	-92	-87	2.35	5.75	-5.44	39	3	1	-80	-42	-41	2.05	14.00	41.00	48	18	1	-88	-61	-52	1.83	3.39	52.00	A	
49	-11	-22	-114	-49	-41	2.32	-4.45	-1.86	51	-3	-8	-128	-67	-62	2.51	-22.33	-7.75	61	10	-9	-146	-97	-75	2.40	9.70	-8.33	S <sub>1</sub>	
57	-3	-8	-131	-70	-62	2.30	-23.33	-7.75	60	11	1	-148	-99	-82	2.47	9.00	82.00	74	27	12	-180	-128	-110	2.43	4.74	9.17	B	
64	13	0	-158	-109	-94	2.47	8.38	∞	66	19	5	-180	-129	-106	2.73	6.79	21.20	77	36	18	-208	-160	-138	2.70	4.45	7.66	C	
85	45	22	-252	-216	-171	2.96	4.80	7.77	85	54	23	-272	-241	-157	3.20	4.46	6.83	96	65	38	-310	-273	-204	3.13	4.20	5.37	D	
64	30	14	-203	-173	-141	3.17	5.77	10.07	64	38	18	-225	-199	-150	3.52	5.24	3.33	72	50	26	-250	-227	-177	3.47	4.54	6.81	E	
31	13	6	-73	-62	-52	2.36	4.77	8.67	25	10	5	-71	-61	-55	2.84	6.10	11.00	27	17	8	-76	-69	-63	2.82	4.06	7.88	F	
10	5	2	-15	-13	-10	1.50	2.60	5.00	8	2	2	-15	-13	-15	1.87	6.50	7.50	10	7	3	-18	-16	-13	1.80	2.29	4.33	G	
45	1	-15	-110	-53	-28	2.44	53.00	-1.87	53	12	4	-110	-78	-74	2.07	6.50	18.50	60	49	-9	-150	-120	-79	2.50	2.45	-8.78	R <sub>2</sub>	
45	-6	-26	-113	-50	-24	2.51	-8.34	-9.2	52	11	1	-110	-78	-72	2.12	7.08	72.00	58	47	-14	-142	-115	-80	2.45	2.45	-5.72	S <sub>H</sub>	
37	15	4	-113	-70	-45	3.05	4.66	11.25	29	12	8	-104	-83	-79	3.58	6.92	9.88	33	21	10	-127	-106	-89	3.85	5.05	8.90	H	
41	15	-2	-122	-103	-71	2.98	6.87	-35.50	39	11	5	-128	-111	-107	3.28	10.09	21.40	42	31	8	-152	-133	-120	3.62	4.29	15.00	R <sub>1</sub>	
41	14	4	-122	-103	-92	2.98	7.35	23.00	35	14	11	-128	-119	-118	3.66	8.50	10.72	38	23	12	-146	-135	-127	3.84	5.87	10.59	K	
56	26	19	-197	-166	-158	3.52	6.38	8.31	57	32	17	-226	-202	-154	3.97	6.31	9.06	62	47	30	-250	-241	-198	4.03	5.13	6.60	L	
50	32	21	-182	-174	-157	3.64	5.44	1.48	49	34	18	-204	-195	-150	4.16	5.74	8.33	51	47	29	-215	-230	-190	4.22	4.90	6.55	M	
30	18	13	-94	-92	-90	3.13	5.11	6.92	26	18	14	-98	-100	-96	3.77	5.55	6.85	31	28	21	-116	-122	-122	3.74	4.35	5.81	N	
12	5	2	-26	-24	-24	2.17	4.80	12.00	9	6	1	-29	-30	-25	3.22	5.00	25.00	8	8	4	-31	-31	-28	3.87	3.87	7.00		

Run 47 (air speed 103 m. p. h. <sup>1</sup> )									Run 48 (air speed 117 m. p. h. <sup>1</sup> )									Run 49 (air speed 125 m. p. h. <sup>1</sup> )									Time, sec.	Rib		
Rib load, lb.			Rib moment, lb.-ft.			c. p. from lead- ing edge, ft.			Rib load, lb.			Rib moment, lb.-ft.			c. p. from lead- ing edge, ft.			Rib load, lb.			Rib moment, lb.-ft.			c. p. from lead- ing edge, ft.						
1.75	2.50	3.10	1.75	2.50	3.10	1.75	2.50	3.10	1.08	1.92	2.60	1.08	1.92	2.60	1.08	1.92	2.60	1.60	2.10	2.90	1.60	2.10	2.90	1.60	2.10	2.90				
62	46	20	-136	-112	-88	2.20	2.44	4.40	78	66	-1	-181	-164	-125	2.32	2.48	-125.00	76	72	22	-186	-179	-131	2.45	2.49	5.95	S <sub>B</sub>			
60	44	19	-127	-103	-79	2.12	2.34	4.16	78	66	-3	-171	-154	-115	2.20	2.34	-38.30	75	71	22	-174	-167	-122	2.32	2.35	5.55	S <sub>1</sub>			
66	50	26	-122	-98	-74	1.85	1.96	2.84	66	54	-3	-152	-135	-95	2.30	2.50	-31.70	73	69	26	-152	-145	-100	2.08	2.10	3.85	S <sub>4</sub>			
73	57	34	-111	-87	-63	1.52	1.52	1.85	84	72	22	-134	-117	-82	1.59	1.62	3.73	86	82	45	-135	-128	-87	1.57	1.56	1.93	S <sub>3</sub>			
79	63	41	-121	-97	-73	1.53	1.54	1.78	72	60	33	-119	-102	-71	1.65	1.70	2.15	83	79	46	-137	-130	-89	1.65	1.65	1.93	S <sub>2</sub>			
88	72	50	-143	-119	-95	1.62	1.65	1.90	87	75	42	-162	-145	-112	1.86	1.93	2.67	91	87	58	-157	-150	-114	1.73	1.72	1.97	A			
100	83	61	-169	-146	-121	1.69	1.76	1.98	99	86	54	-183	-166	-137	1.85	1.93	2.54	106	102	72	-199	-191	-155	1.88	1.87	2.15	S <sub>1</sub>			
106	88	61	-183	-164	-130	1.73	1.87	2.13	108	91	61	-203	-182	-159	1.88	2.00	2.61	115	111	77	-217	-211	-175	1.88	1.90	2.27	B			
87	64	41	-121	-104	-81	1.39	1.63	1.98	86	64	37	-135	-116	-103	1.57	1.81	2.79	93	83	52	-147	-134	-107	1.58	1.61	2.06	C			
54	29	3	-34	-3	16	.63	.10	-5.33	56	25	7	-42	0	-4	.75	0	.57	59	41	10	-42	-10	9	.71	.24	-.90	D			
62	37	17	-49	-24	1	.79	.65	-.06	60	34	19	-47	-16	-23	.78	.47	1.21	62	53	24	-47	-36	-9	.76	.68	.37	E			
66	43	26	-96	-68	-51	1.45	1.58	1.96	67	46	26	-99	-76	-62	1.47	1.65	2.38	74	61	37	-111	-96	-68	1.50	1.57	1.83	F			
41	27	14	-45	-33	-19	1.10	1.22	1.36	39	26	12	-43	-32	-22	1.10	1.23	1.83	42	35	19	-45	-40	-24	1.07	1.14	1.26	G			
76	32	-3	-169	-101	-76	2.22	3.16	-25.33	50	29	9	-149	-121	-118	2.98	4.17	13.10	55	36	29	-169	-136	-128	3.07	3.78	4.41	R <sub>2</sub>			
74	29	-6	-143	-75	-53	1.93	2.58	-8.84	50	28	5	-137	-101	-90	2.74	3.61	18.00	55	34	21	-157	-124	-100	2.85	3.65	4.77	S <sub>H</sub>			
51	4	-20	-141	-72	-50	2.76	18.00	-2.50	48	7	-21	-145	-99	-74	3.02	4.10	-3.52	51	23	-3	-161	-129	-99	3.16	5.61	-33.00	H			
65	15	-13	-156	-87	-60	2.40	5.80	-4.62	59	20	-12	-156	-110	-85	2.64	5.50	-7.08	62	34	5	-172	-139	-106	2.77	4.09	21.20	R <sub>1</sub>			
59	21	-1	-117	-67	-43	1.98	3.19	-43.00	59	21	4	-134	-84	-81	2.27	4.00	20.20	63	42	10	-146	-116	-79	2.32	2.76	7.90	J			
46	18	-2	-42	-10	8	.91	.55	4.00	43	15	1	-49	-12	-18	1.14	.80	18.00	45	29	1	-51	-24	1	1.13	.83	-1.00	K			
49	18	0	-39	2	20	.80	-.11	∞	47	18	1	-37	0	3	.79	0	-3.00	50	38	8	-43	-31	11	.86	.82	-1.37	L			
64	39	22	-101	-71	-50	1.58	1.82	2.27	67	43	26	-112	-81	-73	1.67	1.88	2.81	73	59	36	-123	-106	-77	1.69	1.80	2.14	M			
45	28	13	-56	-38	-22	1.24	1.35	1.69	45	28	16	-57	-39	-30	1.26	1.39	1.87	51	41	22	-64	-53	-34	1.25	1.29	1.54	N			





Positive directions of axes and angles (forces and moments) are shown by arrows

Axis		Force (parallel to axis) symbol	Moment about axis			Angle		Velocities	
Designation	Sym- bol		Designation	Sym- bol	Positive direction	Designa- tion	Sym- bol	Linear (compo- nent along axis)	Angular
Longitudinal	X	X	Rolling	L	Y→Z	Roll	φ	u	p
Lateral	Y	Y	Pitching	M	Z→X	Pitch	θ	v	q
Normal	Z	Z	Yawing	N	X→Y	Yaw	ψ	w	r

Absolute coefficients of moment

$$C_l = \frac{L}{qbS}$$

(rolling)

$$C_m = \frac{M}{qcS}$$

(pitching)

$$C_n = \frac{N}{qbS}$$

(yawing)

Angle of set of control surface (relative to neutral position), δ. (Indicate surface by proper subscript.)

#### 4. PROPELLER SYMBOLS

D, Diameter  
p, Geometric pitch  
p/D, Pitch ratio  
V', Inflow velocity  
V<sub>s</sub>, Slipstream velocity

T, Thrust, absolute coefficient  $C_T = \frac{T}{\rho n^2 D^4}$

Q, Torque, absolute coefficient  $C_Q = \frac{Q}{\rho n^2 D^5}$

P, Power, absolute coefficient  $C_P = \frac{P}{\rho n^3 D^5}$

C<sub>s</sub>, Speed-power coefficient =  $\sqrt[5]{\frac{\rho V^5}{P n^2}}$

η, Efficiency

n, Revolutions per second, r.p.s.

Φ, Effective helix angle =  $\tan^{-1} \left( \frac{V}{2\pi r n} \right)$

#### 5. NUMERICAL RELATIONS

1 hp. = 76.04 kg-m/s = 550 ft-lb./sec.

1 metric horsepower = 1.0132 hp.

1 m.p.h. = 0.4470 m.p.s.

1 m.p.s. = 2.2369 m.p.h.

1 lb. = 0.4536 kg.

1 kg = 2.2046 lb.

1 mi. = 1,609.35 m = 5,280 ft.

1 m = 3.2808 ft.